3D-Printed Membrane as an Alternative to Amniotic Membrane for Ocular Surface/Conjunctival Defect Reconstruction: An In Vitro & In Vivo Study

Shima Dehghani[1], Morteza Rasoulianboroujeni[2], Hamed Ghasemi[1,*], Saeed Heidari Keshel[1], Zohreh Nozarian[1], Mohammad Naser Hashemian[1], Mehran Zarei-Ghanavati[1], Golshan Latifi[1], Reza Ghaffari[1], Zhanfeng Cui[3], Hua Ye[3,*], Lobat Tayebi[2,3,*]

[1] Eye Research Center, Farabi Eye Hospital, Tehran University of Medical Sciences, Tehran, Iran

[2] Marquette University School of Dentistry, Milwaukee, WI 53233, USA

[3] Institute of Biomedical Engineering, Department of Engineering Science, University of Oxford, Oxford OX1 3PJ, UK

Corresponding Authors:

Hamed Ghassemi, Eye Research Center, Farabi Eye Hospital, Tehran University of Medical Sciences, Tehran, Iran.

Email: h_ghassemi@sina.tums.ac.ir

Hua Ye, Institute of Biomedical Engineering, Department of Engineering Science, University of Oxford, Oxford OX1 3PJ, UK

Email: hua.ye@eng.ox.ac.uk

Lobat Tayebi, Marquette University School of Dentistry, Milwaukee, WI, USA

Email: lobat.tayebi@marquette.edu

Abstract

Background: The aim of this study was to evaluate the surgical handling and clinical applicability of a specific 3D-printed membrane design fabricated using a gelatin, elastin and sodium hyaluronate blend for conjunctival reconstruction and compare it with amniotic membrane (AM), which is normally used in such surgeries.

Methods: 3D printing technique was employed to fabricate the membrane based on gradient design. Prior to printing, rheometry was employed to optimize the ink composition. The printed membranes were then fully characterized in terms of physical and mechanical properties. In vitro viability, proliferation and adhesion of human limbal epithelial cells were assessed using MTT assay and scanning electron microscopy (SEM), respectively. Prior to in vivo experiment, surgical handling of each membrane was evaluated by three surgeons. In vivo evaluation was conducted through implanting the gelatin-based membranes and AM on induced conjunctival defects in rabbits (n=8). Clinical observations, including epithelialization, inflammation severity, scar tissue formation and presence of granulation tissue, were recorded from day 1 through day 28. Histological examination was performed on all enucleated eyes on day 28. In addition to H&E staining, specific stains including Periodic Acid Schiff staining, Masson's Trichrome staining and immuno-histochemical staining for α-SMA were further used to assess goblet cell proliferation, healed sub-epithelial stroma and scar tissue formation and the presence of myofibroblasts, respectively.

Results: Among all the examined compositions, a blend of 8% w/v gelatin, 2% w/v elastin and 0.5% w/v sodium hyaluronate was found to be appropriate for printing. The printed membranes had favorable optical characteristics (colorless and transparent), and the surgical handling was significantly easier compared to AM. Epithelial cells cultivated on the membranes indicated suitable viability and proliferation, and SEM images presented appropriate cell adhesion on the surface of the membranes. Clinical observations suggested similar epithelialization time (approximately 3 weeks) for both the membrane and AM grafted eyes but significantly lower levels of clinical inflammation in the membrane group from day 1 through day 28 ($p = 0.01$), which is a key advantage of using the printed membranes over the AM. Histological examination showed similar qualities in the healed epithelium in terms of cell morphology and cell layers. However, twice the density of goblet cells per 100 cells was observed in the gelatin-based membrane grafted group. Remnant of the degraded implant was seen in only 3 of the membranes, but in 7 of the AM grafted eyes. Inflammation and granulomatous reaction was significantly higher in sections containing the AM compared to

membrane ($p < 0.01$ and $p = 0.01$, respectively). α-SMA staining was more evident, but not significantly different from the gelatin-based membrane, for the AM group ($p = 0.25$).

Conclusion: The designed gelatin-based membrane offers the necessary physical and mechanical characteristics needed for successful ocular surface/conjunctival defect construction and may be considered a promising alternative to AM due to a more predictable degradation pattern, higher goblet cell density on the healed epithelium, less inflammation and reduced scar tissue formation.

Keywords: Conjunctival Reconstruction; Conjunctival Defect; Amniotic Membrane; Gelatin-Based Membrane; Ocular Surface Regeneration; 3D Printing

1. Introduction

Ocular surface damage can occur due to various reasons, such as ocular thermal/chemical burns [1], autoimmune diseases (Steven Johnson's, ocular cicatricial pemphigoid) [2, 3], or due to iatrogenic causes during surgeries where conjunctival excision is necessary, such as Pterygium surgery [4] and conjunctival tumor removal [5]. Repair of the damaged or absent conjunctivae is of utmost importance, as conjunctivae is necessary for proper function of the ocular refractive surface and protection of the cornea. The latter is accomplished through equilibrium of the tear film composition by secreting aqueous, lipid and mucin [6]. The conjunctiva also plays a role in protecting the eye from microbial infections by acting as a mechanical barrier and containing lymphoid tissue (conjunctiva-associated lymphoid tissue—CALT) [7]. Although re-epithelization will occur spontaneously upon conjunctival injury [8-10], several limitations including reduced goblet cell density, scar tissue formation and contracture hinder the function and anatomy of the healed epithelium that may eventually lead to unfavorable results and even blindness. Goblet cell density and, consequently, the mucin layer thickness of the tear film, that is essential for maintaining the wettability of the ocular surface and clearing it of debris [11], decrease with injury in the healed epithelium [9, 12]. On the other hand, conjunctival contracture and reduced overall surface may lead to fornix foreshortening and eventual symblepharon formation and entropion in the involved eye [13, 14].

Despite favorable results [14-16], autologous tissues have some limitations to replace the absent conjunctiva or modulate the healing process, including unavailability of healthy conjunctiva in autoimmune diseases, cosmetic issues, and absence of goblets [7]. Therefore, allografts such as pericardium [10] and amniotic membrane (AM) have been introduced. AM currently serves amongst the most widespread grafts used in ocular surface reconstruction. It is currently used as a substitute for excised conjunctivae in pterygium surgery, symblepharon lysis, fornix reconstruction, conjunctivochalasis and in tumor resections [17]. AM has been shown to facilitate epithelialization by providing a basement membrane and stroma resembling that of the normal conjunctivae [2, 14, 18, 19]. Studies have also mentioned anti-inflammatory and anti-fibrotic properties, along with lack of immunogenicity for AM [20, 21]. The mentioned characteristics have made AM a favorable tissue for ophthalmic applications [22, 23]. However, there are some studies that challenge the preferential use of AM. For example, histological examinations showed low levels of epithelial stratification (single) and low goblet density (sparse PAS positive cells) on the epithelium grown on cultured AM [24]. Despite favorable results on suppression of inflammation by AM reported in prior studies [1, 2, 14, 18, 21, 25-27], there have been some evidence showing increased inflammatory response in

histological sections of wounds grafted with AM [10, 28-30] after conjunctival reconstruction with human AM. Moreover, considering that AM is an allogenic tissue, limitations in the number of diseases that it can be screened for remains a concern [22]. Another complication associated with AM is the considerable likelihood of microbial infections and unwanted host reactions due to lack of standardized and sterile tissue preparations. Post AM transplantation rate of infection (culture positive) has been reported to be 3.4% in a study on 326 patients [31]. Difficult surgical handling (notably suturing due to the thin structure of AM), prolonged presence in the AM graft site [13, 28, 29], and opacification of the site [32] are among other reported issues associated with AM. Such limitations necessitate development of efficient alternatives like bioengineered scaffolds that can have stroma-like structure similar to AM, promote epithelialization while not transmitting allogenic-related diseases. The results of animal study of several synthetic materials including collagen-glycosaminoglycan (CG) copolymer [9], poly (lactide-co-glycolide) (PLGA) [8], vitrified collagen [12], and cultured membranes [30, 33] have been promising in terms of successful re-epithelialization, decreasing scar formation and fornix foreshortening [13, 18, 19]. However, they still have limitations like undesirable transparency, elasticity, and thickness [8-10]. Also, the ease of surgical handling and the goblet population have not been thoroughly discussed [8, 9, 34]. Among different biomaterials, biodegradability, biocompatibility, ease of processing, and relative inexpensiveness of gelatin-based ones have been the main drivers for further studies, albeit predominantly preclinical, on their ocular applications. Although gelatin-based constructs have been extensively investigated over the last few decades for a multitude of ocular applications [35-42], conjunctival reconstruction has not been reported as a potential application for this group of biomaterials despite their favorable characteristics mentioned above.

This paper is aimed at the development and application of a 3D-printed gelatin/elastin/hyaluronic acid membrane for conjunctival reconstruction and evaluation of epithelialization (time to epithelialization and morphology of the healed epithelium), goblet cell morphology and density, degree and type of inflammation (clinical and histological assessment), quality of healed sub-epithelial stroma and scar tissue formation (gross tissue deformation, collagen deposition pattern from histological data, myofibroblasts by immune histochemical stationing for α-SMA). Additionally, results of the evaluation conducted on the fabricated membrane were compared with corresponding evaluation for the widely used AM graft. Prior to in vivo tests conducted on animal models, the membranes were tested for in vitro biocompatibility as well.

2. Experimental Procedure

2.1. Ink Formulation

The ink used in this study was composed of gelatin (Type A, from porcine skin, Bioreagent grade, Sigma, US), soluble elastin (MW 60KDa, Elastin Products Company, Inc., USA) and sodium hyaluronate (Research Grade, 500KDa-749KDa, Lifecore Biomedical, USA). Gelatin was used as the main component of the ink, while elastin and sodium hyaluronate were employed as additives. Rheological measurements were used to characterize various ink formulations listed in Table 1.

Table 1: Detailed composition of various formulations used for rheological measurements.

Ink ID	Gelatin concentration (%w/v)	Elastin concentration (%w/v)	Sodium hyaluronate concentration (%w/v)
G4	4	-	-
G8	8	-	-
G16	16	-	-
G4E2	4	2	-
G8E2	8	2	-
G16E2	16	2	-
G4E2H0.5	4	2	0.5
G8E2H0.5	8	2	0.5
G16E2H0.5	16	2	0.5

The gelation temperature of each formulation was determined using oscillatory shear measurements. A shear rheometer (Kinexus, Malvern, UK) with a stainless steel parallel-plate geometry of 20 mm in diameter and a Peltier temperature control was used to perform frequency sweep at the gap distance of 0.3 mm for each formulation at temperatures in decreasing 2 °C increments starting from a certain temperature above the formulation gelation temperature. A constant shear strain of 0.1% was applied to each sample during the frequency sweep, where the sample deformation was well within the linear viscoelastic region. The formulation with the sol-gel transition temperature closest to room temperature was selected for printing.

The creep test was run for the selected formulation and the corresponding gelatin solution with no additives. The measurements were conducted at the constant shear stress of 10 Pa using the same parallel-plate geometry and gap distance as the oscillatory measurements at 24-32 °C. Both creep and recovery phases were monitored for up to 10 min unless the equilibrium condition for steady state was met.

The viscometry of the samples was conducted using the same geometry and gap distance at temperatures in decreasing 2 °C increments ranging from 36 °C to 26 °C. The shear rate varied logarithmically in ramp mode from 0 to 50 s^{-1} and then back to 0 s^{-1}.

2.2. 3D-printing of Membranes

The mass flow of the selected ink as a function of actual pneumatic pressure applied by the printer to the ink reservoir was obtained by holding the pressure for 30 s and weighing the dispensed material. Two different needles with inner diameters of 250 (G25) and 410 μm (G22) were examined while the reservoir temperature was set to either 32 or 34 °C. The effect of cooling rate and ultimate temperature on the rheological properties of the selected ink was also investigated. For this purpose, the same parallel-plate geometry with a gap distance of 0.2 or 0.4 μm was employed. The initial temperature was set to 32 °C, and the measurements were conducted in oscillatory mode with a shear strain of 0.1% and a frequency of 1 Hz. The temperature was decreased to 12, 18 or 24 °C, with a cooling rate of 10, 8 or 4 °C/min, respectively, while the oscillatory measurement was current. The variation of complex shear modulus against time was then plotted to evaluate the effect of various temperatures and cooling rates on the kinetics of hardening.

The final membranes were fabricated using a 3D-bioplatter (EnvisionTEC, Germany). Taking the rheology analysis into account, the selected solution was printed at material container temperature of 32 °C, platform temperature of 12 °C, printing pressure of 0.7 bar, and speed of 20 mm/s using a 250 μm-diameter needle. Pre- and post-flow delays were set to zero. Each membrane was composed of 6 layers with strand angles of 45, 135, 0, 90, 0 and 90°. Distances between strands were set to 0.6 μm for the first 4 layers and 0.9 μm for the last 2 layers. Hardening of the ink occurred after being dispensed from the needle and touching the platform through the capability of the solution to form a solid gel at lower temperatures. The samples were cross-linked using 6 mg/ml 1-ethyl-3-(3-dimethylaminopropyl)carbodiimide hydrochloride (EDC, Alfa Aesar, USA)/ 0.75 mg/ml N-hydroxysulfosuccinimide (NHS, Alfa Aesar, USA) in 70% (v/v) ethanol for 1.5 h (see supplementary information, cross-linking section), washed with a large amount of DI water and stored in pure ethanol (dehydrated state) at -20 °C until use.

2.3. Morphology, Line and Surface Roughness

Morphology, line and surface roughness of the membranes were evaluated using a 3D Laser Measuring Microscope (LEXT OLS4000, Olympus, Japan). Samples were imaged both in dehydrated (stored in ethanol) and hydrated states. The arithmetic average of the absolute values of the profile height deviations from the mean line (R_a) and the mean surface (S_a) were used to describe line and surface roughness, respectively.

2.4. Human AM Preparation and Preservation

Cryopreserved human AM (commercialized as *Life Patch* by International Bio Implant (IBI) Company, Tehran, IR) was used in this study. The manufacturer reported that these AMs were partially acellular, DNA diminished, lacking MHC expression, and kept in a solution containing antibiotics (vancomycin, gentamycin, ceftriaxone, streptomycin, glucosulin, and amphotericin B). AMs were stored at -20 ˚C. All donors and AMs processed at IBI were screened against human immunodeficiency virus type 1 and 2, human T-lymphocyte virus type 1 and 2, hepatitis B and C viruses, and syphilis both at delivery and at the time of preparation. Further details pertinent to preparation procedure were not disclosed by the manufacturer due to proprietary concerns. a total of 4 AMs were used in this study. AMs were defrosted in room temperature for 10 minutes prior to use. Then, the plastic paper was peeled off and the AMs were washed in balanced saline solution.

2.5. In-Vitro Cell Viability and Attachment Evaluation

2.5.1. Human limbal epithelial cell isolation and culture

Healthy human limbal tissues (2 mm length and from superior limbus) were transferred immediately to the laboratory using a special media containing Hank's balanced salt solution (HBSS), amphotericin B, and penicillin/streptomycin (all three: Gibco, Massachusetts, USA), at 4 °C. Limbal epithelial progenitor cells (LEPCs) were isolated by using mechanical and enzymatic processes under sterile conditions as follows:

The samples were first cut into smaller pieces and incubated in 10 mM dispase II for 2 hours at 37 °C. Following isolation of the epithelial layer, the limbal samples were incubated in collagenase II for 20 minutes at room temperature and treated with cold trypsin for 10 minutes at 37 °C. The specimens were then centrifuged (400 g at 4 °C). Lastly, the collected cells were suspended in supplemental hormonal epithelial medium (SHEM) and cultured in cell culture plates. To cultivate limbal epithelial cells (SHEM), a mixture of DMEM/F12 (Gibco, Massachusetts, USA; 1:1) was used and supplemented with 10% human serum, 1.05 mM calcium, 5 µg/ml crystalline bovine insulin, 30 ng/ml cholera-toxin, 2 ng/ml epidermal growth factor (EGF), 0.5% dimethyl sulfoxide (DMSO; all from Sigma Chemical Co, St. Louis, USA), 0.5 µg/ml hydrocortisone (Gibco, Massachusetts, USA) , 5 ng/ml sodium selenite (Gibco, Massachusetts, USA), and 5 µg/ml apo-transferrin (Gibco, Massachusetts, USA). Adherent epithelial cells were separated after 3 weeks.

2.5.2. Cell attachment and proliferation assays

MTT assay was used to assess cell viability and proliferation on the proposed membrane. Among the enzyme-based assays, MTT assay is the best-known method for determining

mitochondrial dehydrogenase activities in living cells. Enzyme-based methods rely on a reductive coloring reagent and dehydrogenase in a viable cell to determine cell viability with a colorimetric method. These methods are superior to others since they are easy-to-use, safe, highly reproducible, and widely used in both cell viability and cytotoxicity tests.

Human limbal epithelial progenitor cells (LEPCs) at a plating density of 5×10^3 cells/well were seeded onto membranes in 96 well plate cell cultures. For the analysis of proliferation rate and viability after 24, 48, 72 hours of culture, 20 µL of MTT (Sigma, US) substrate (of a 2.5 mg/ml stock solution in phosphate-buffered saline) was added to each well, and then all the plates were returned to standard tissue incubator conditions for an additional 4 hours, after which, the medium was removed, and the cells were solubilized in 100 µL of dimethyl sulfoxide (DMSO, Sigma, US) in preparation for the colorimetric analysis (wavelength, 570 nm, PHOMO microplate reader).

2.6. Mechanical Properties, Suturability and Assessment of Surgical Handling of the Membranes

To quantify the mechanical properties and suturability of the gelatin-based membranes, a universal testing machine (UTM, Shimadzu, Japan) was employed. Membranes were examined in terms of Young's modulus, ultimate strength and the suture retention strength. To do this, membranes were fixed in the lower clamp of the machine; a standard steel wire (D = 0.3 mm) was punctured through the membrane and the two ends were enclosed within the upper clamp to form a ring-like structure. Suture pullout was conducted by moving the upper clamp with the force being monitored. The mechanical tests were conducted using a 1 kN load cell and a crosshead speed of 1 mm/min.

The objectivity of the surgical handling assessment was ensured by assigning three different surgeons with subspecialty in Cornea and Ocular Surface to conduct the operations. Surgeons did not have any prior knowledge about the make and composition of the scaffolds to mitigate the bias in their evaluations. The assessment comprised of suturability, ease of manipulation and cutting with surgical forceps and scissor, and rigidity in terms of how the scaffold lied on the tissue. Surgical operations were recorded (see supplementary data for the videos). Comparative evaluation of the surgical handling of GM versus AM was also done by recording and evaluating in-vivo operations (details are provided in section 2.7).

2.7. Conjunctival Defect Induction and AM/Gelatin-Based Membrane Implantation in Rabbit Models

The study included ten male albino rabbits weighing between 3 and 4 kg. The rabbits were all treated according to national guidelines. All investigations conformed to the ARVO Statement for the Use of Animals in Ophthalmic and Vision Research and were approved by Tehran University of Medical Sciences. Eight rabbits were used as the study group. Induced conjunctival defects were transplanted with gelatin-based membrane in one eye and AM in the contralateral eye. The remaining two rabbits served as the control group and were left ungrafted (bare) after conjunctival excision, in only one eye. All surgeries were performed by the same surgeon with the aid of a surgical microscope. The rabbits were first anesthetized by intramuscular injection of ketamine (15 mg/kg) and xylazine (5 mg/kg). The eyelids were held open during surgery by a speculum.

The defect location was first marked by 8 mm vacuum trephine, colored with surgical ink at the edge, on the supra-temporal conjunctiva of both eyes of each rabbit. The conjunctiva and Tenon were excised with Vannas scissors to the level of bare sclera, ensuring that no Tenon remained. All defects maintained a 2 mm distance from the corneal limbus. Special care was exercised so that the induced defects only involved the bulbar conjunctivae and were not extended into the forniceal area. The use of anchoring sutures, required in surgeries involving fornix reconstruction, was not within the scope of this study.

The gelatin-based membrane and AM were marked with the same vacuum trephine as described above and cut into 8 mm round pieces with Vannas scissors. The AM (epithelium side up) and gelatin-based membrane were secured to episclera with four Nylon 6.0 (Supa, Tehran, IR) sutures (one at the limbal and the other at the forniceal side of the defect) to prevent dislodging, and the remaining surface was adhered to the bare sclera with fibrin glue (Beriplast® P Combi Set, CSL Behring, USA). Both implants covered the bare area completely. The edges of the conjunctivae were slightly pulled to meet the edges of the membranes or AM (Figure 1). Eyes in the control group were left ungrafted, without any further manipulation. Chloramphenicol and betamethasone (Sina Darou, Tehran, IR) eye drops were instilled in the eyes of all rabbits immediately after surgery and then twice a day afterwards for 4 weeks.

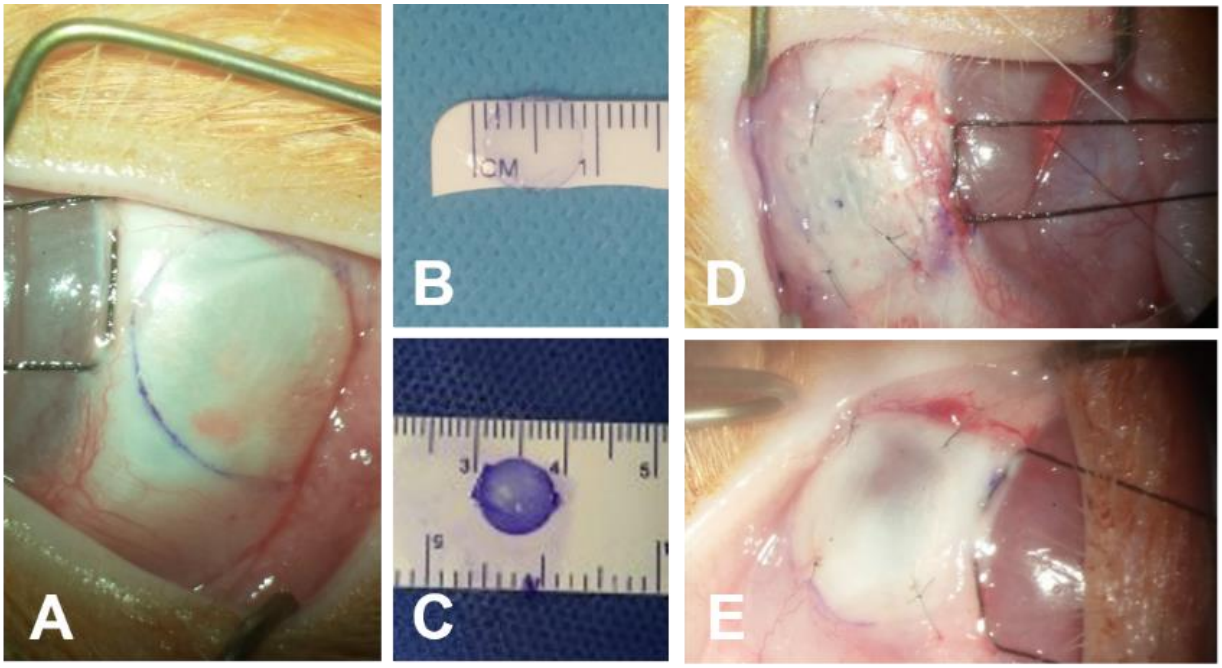

Figure 1. Induction of conjunctival defect and implantation of membranes. (A) The final defect, (B) Gelatin-based membrane, (C) AM cut into an 8-mm round piece, (D) Representative eye implanted with Gelatin-based membrane, (E) Representative eye grafted with AM.

2.8. Clinical Observations

All rabbits were examined and photographed on days 1, 7, 14, 21 and 28 post-surgery. During examinations, the defect size and epithelialization extent were investigated via fluorescein staining under cobalt blue light. Inflammation severity (rated as mild, moderate, or severe, based on the degree of conjunctival hyperemia and vessel engorgement) and discharge were probed. The scar tissue formation was qualitatively assessed based on gross clinical observations (in terms of conjunctival contracture, vascular pattern alteration, scleral vessel obscuration, and the appearance of fibrous tissue). The presence of granulation tissue or symblepharon were also recorded. Each rabbit was examined by two ophthalmologists independently (i.e. the surgeon and another ophthalmologist who was blind towards the study groups). All observations were double checked.

2.9. Histological Staining

All 14 rabbits were sacrificed on day 28. Intact eyes, including forniceal and palpebral conjunctivae, were removed via orbital enucleation by the same initial surgeon, and then fixed via immersion in 10% formaldehyde and transferred to the pathology department. Sections were

obtained from the center and edges of each healed defect. All dissections were done in the presence of the surgeon to ensure that the exact defective site was included. Sections were then embedded in paraffin, cut into 5 micrometer thick layers using a microtome, and stained with Hematoxylin and Eosin (H&E) for general tissue morphology. Further and more specific staining was performed in order to evaluate goblet cell density and collagen alignment, as discussed in sections 2.9.2 and 2.9.3. Each specimen was observed under 100X and 400X magnifications by a pathologist who was blind towards the treatment groups. All observations were then double checked in the presence of the surgeon.

2.9.1. H&E staining

Epithelialization was recorded as the presence or absence of a continuous layer of epithelium at the defective site. The quality of the healed epithelium was further assessed by recording the number of epithelial layers, representing stratification, and the flattening of epithelial cells while migrating towards the superficial epithelial layers. The inflammation was quantitatively recorded based on the average density of the inflammatory cells observed in each power field. In doing so, the following grading was used: (0) none, (1) mild, (2) moderate, and (3) severe. The inflammation was further classified as granulomatous and non-granulomatous based on the presence of giant cells and histiocytes at the healed defective site or surrounding the transplant.

2.9.2. Periodic Acid Schiff (PAS) staining

All tissue sections were stained with PAS and characterized in terms of goblet cell morphology and density (i.e. goblet cell count in any group of 100 cells within the epithelium). After characterization, the stained tissue sections were divided into two groups, including one with sections with less than 10% goblet cell density and one with those equal to or more than 10% density.

2.9.3. Masson's Trichrome (MT) staining

In order to evaluate the quality of healed sub-epithelial stroma, all sections were additionally stained with MT to observe collagen fibril alignment. The observed quality was rated as follows: (1) randomly aligned and loose collagen deposition, or (2) parallel and packed collagen deposition. Sub-epithelial fibrosis was considered to be present if a packed and parallel collagen alignment, stained blue with MT, was observed in the sub-epithelial area.

2.9.4. Immunohistochemical staining for alpha-Smooth Muscle Actin (α-SMA)

The presence or absence of α-SMA was recorded in each power field. The higher density of myofibroblasts served as an indicator of a higher possibility for tissue contraction in the future.

2.10. Statistical Analysis

The raw data was analyzed using Statistical Product and Service Solutions (SPSS) v25.0 software. The normality of data distribution was checked using the Kolmogorov-Smirnov test. The Fisher's exact test was performed to compare categorical data of three groups under investigation. The continuous data of the groups were compared using Kruskal Wallis analysis. All reported *p*-values were two-sided. The inferences were considered to be statistically significant when the *p*-values were less than 0.01.

3. Results and Discussion

3.1. Ink Formulation and 3D-Printing of the Membranes

The ink employed in this study was composed of gelatin, elastin and sodium hyaluronate. Gelatin sol-gel transition plays an important role in the printing procedure as it might be both in favor of or against successful printing. While it assists the ink hardening on the platform and shape fidelity of the printed strands, it might cause obstruction of the dispensing needle and interruption of printing. The sol-gel transition temperature of each individual formulation was determined as the frequency-independent value of the damping factor (tan δ) obtained from a multi-frequency plot for a temperature sweep measurement [43] (see supplementary information Fig. S1).

The sol-gel transition temperature was found to be around 22, 24 and 28 °C for 4, 8, 16% (w/v) aqueous solution of gelatin (G4, G8 and G16), respectively (Fig. S1). Addition of both elastin and sodium hyaluronate had a minor effect on the gelation temperature, except in the case of G4E2H0.5 where the sol-gel transition could not be detected. In our formulation, gelatin is known to form a thermally reversible physical network when cooled through local assembly of protein coils into triple helices dominated by hydrogen bonding [44]. Our data suggests that there is no significant complexation between sodium hyaluronate and gelatin molecules, which is in agreement with the isothermal microtitration calorimetry results obtained by Picard et al. [45]. It has been reported that the extent of triple helix formation in gelatin-hyaluronic acid mixtures is independent of hyaluronic acid concentration, suggesting that unlike some vegetal polysaccharides such as inulin, arabic gum or guar gum [46], hyaluronic acid does not influence network formation in the physical gelatin gel [45].

Amongst all the formulations containing gelatin, elastin and sodium hyaluronate, the sol-gel transition temperature of G8E2H0.5 was found to be close to room temperature. Using such an ink, the obstruction of the dispensing needle that is in contact with ambient temperature can be avoided, while hardening of the ink can be achieved by adjusting the platform temperature well below the room temperature. This formulation was selected to be further characterized and then printed.

In addition to the method proposed by Winter and Chambon [47], the critical gelation point of G8 and G8E2H0.5 samples were determined through plotting the apparent viscoelastic relaxation exponents n' and n" ($G' \propto \omega^{n'}$, $G'' \propto \omega^{n''}$) obtained from the frequency dependence of storage (G') and loss (G") moduli at each temperature (see supplementary information Fig. S2A, B, D, E) against temperature to track a crossover where n' = n" = n (as shown in Fig. S2C, F). While the two methods of determination of critical gelation temperature delivered very close values (~ 24 °C), the latter suggests a slightly lower gelation temperature for G8E2H0.5 compared to G8.

To further examine the effect of additives and to choose appropriate cartridge temperature, creep and recovery tests at different temperatures were performed. The applied stress was bigger than the yield stress of the gel at the lowest examined temperature. As seen in Fig. 2A, G8 and G8E2H0.5 showed a very similar viscoelastic liquid behavior at 20 °C, which is well below the gelation temperature of both. This finding suggests that the elasticity of the gel determined from the total recoverable deformation is mainly governed by gelatin and, consequently, helices content as discussed before. Despite huge similarity, slight differences can be observed in terms of non-recoverable (J_{NR}) and steady-state compliance (J_e^0), both of which are slightly higher for G8E2H0.5. It is worth mentioning that while a viscoelastic liquid has no equilibrium compliance, for such a material, the creep is the sum of a deformation approaching a constant value (J_e^0), analogous to equilibrium compliance for a viscoelastic solid, plus a viscous flow contribution (t/η_0 where t is the creep time and η_0 is Newtonian viscosity). The steady-state compliance (J_e^0) can be considered as a measure of the elastic deformation during steady flow [48].

At 24 °C (very close to the gelation temperature if not exact), the compliances are one order of magnitude higher than 20 °C and both formulations again displayed viscoelastic liquid behavior (see Fig. 2B). The relatively high instantaneous compliances (J_0) for both formulations contributed to a big non-recoverable deformation. The higher creep compliance and non-recoverable deformation for G8E2H0.5 compared to G8 support the outcome of gelation temperature determination through apparent viscoelastic relaxation exponents for slightly lower gelation temperature of G8E2H0.5. Despite being around 4 °C above the gelation temperature of both formulations, 28 °C cannot be considered as an ideal temperature for printing, again since the formulation represents a viscoelastic

liquid behavior with slight recovery, and the deformation/flow of the material is time-dependent. It can be seen in Fig. 2C that G8E2H0.5 is more resistant to deformation compared to G8, likely because of higher total concentration and presence of high molecular weight sodium hyaluronate. It again supports the assumption that at 24 °C, the higher resistance of G8 to deformation compared to G8E2H0.5 could be because of its prompter gelation. Both formulations represented Newtonian behavior at 32 °C, where the presence of sodium hyaluronate acts as a thickener to increase the resistance to flow (see Fig. 2D). This temperature can be considered as an appropriate temperature or the minimum required temperature for printing. All in all, surrendering the quantitative point of view, the creep behavior of the formulations was very similar, implying the key role of gelatin in the formulation.

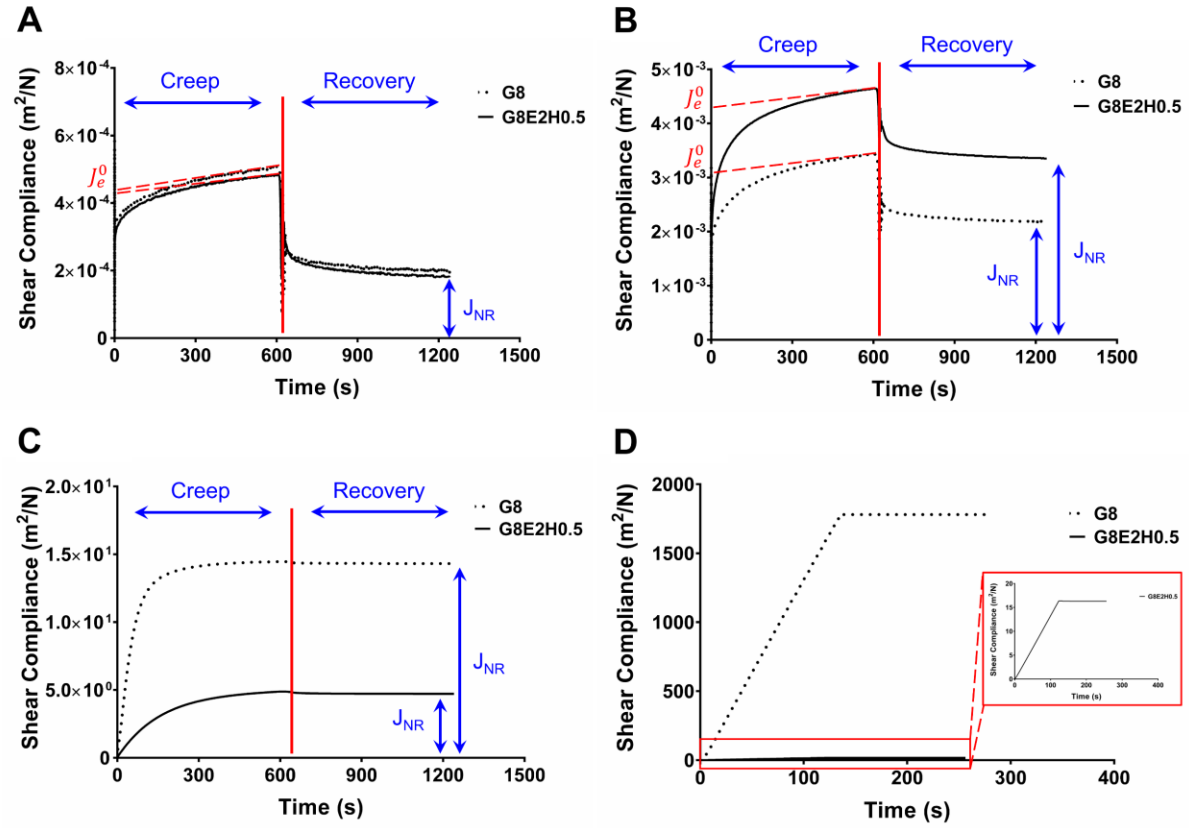

Figure 2. Creep and recovery tests performed at (A) 20 °C, (B) 24 °C, (C) 28 °C and (D) 32 °C for G8 and G8E2H0.5 samples.

Fig. 3A-C shows the shear viscosity of G4E2H0.5, G8E2H0.5 and G16E2H0.5 as a function of shear rate and temperature. Increasing the gelatin concentration had a remarkable effect on the viscosity, particularly at lower temperatures. The viscosity of all the formulations decreased with

increasing temperature, whereas the degree of variation was strongly dependent on gelatin concentration. At lower temperatures (closer to the gelation temperature), the formulations demonstrated shear thinning behavior, whereas at temperatures above 30 °C all behaved nearly Newtonian. Although hyaluronic acid is known to behave as a non-Newtonian and viscoelastic fluid in aqueous solutions [49], both gelatin and hyaluronic acid solutions with concentrations close to the values in our study have been reported to display a Newtonian behavior at elevated temperatures [45]. It has been suggested that the behavior of gelatin-hyaluronic acid mixtures is dictated by the hyaluronic acid, and gelatin only influences the viscosity from a quantitative point of view. As a result, the shear thinning behavior of such mixtures at high shear rates has been hinted to be a result of alignment of polysaccharidic chains in the direction of the flow [45].

Fig. 3D illustrates the mass flow rate of G8E2H0.5 formulation as a function of printer actual pressure at 32 or 34 °C, dispensed using standard 25G (250 μm) or 22G (410 μm) needles. The relationship between the mass flow rate and pressure was nearly linear (coefficient of determination, R^2, greater than 0.9) for both dispensing needles and temperatures. Since the ink represents Newtonian behavior at both temperatures, the Hagen-Poiseuille's equation can be used to correlate the applied pressure and the flow rate as follows:

$$Q = \frac{\pi R^4 \Delta P}{8 \mu l} \qquad \text{Eq. 1}$$

where Q is the flow rate, R is the radius of the pipe, ΔP is the applied pressure, μ is dynamic viscosity and l is the length of the pipe. The linear relationship between the pressure and flow rate, as well as the ratio of the slopes of the lines ($(D_2/D_1)^4$ = 7.23, D_2=410 μm, D_1=250 μm vs. average ratio of the slopes = 7.21), suggests that the flow of the ink through the needle is governed by the Hagen-Poiseuille's equation. Using the G25 needle at 32 °C, the mass flow rate fluctuation caused by varying the applied pressure could be minimized, which is beneficial to the printing procedure, as it reduces the system sensitivity.

Needle obstruction due to ink gelation in the dispensing needle and shape fidelity affected by ink hardening speed on the platform were found to be two important challenges that needed to be addressed to enable successful printing of the membranes. The former was addressed through adjusting the gelation temperature close to the room temperature, while the latter was controlled through cooling the platform. Fig. 3E illustrates the effect of final temperature, cooling rate and the gap distance on the complex shear modulus of G8E2H0.5 as an indicator for the overall resistance to deformation over time when cooled down from 32 °C using a parallel plate geometry in the

rheometer. Indeed, altering the gap distance is expected to affect the heat loss by varying the surface area to volume ratio. Surface area to volume ratio is inversely proportional to the gap distance and diameter of the dispending needle, as halving either one doubles the ratio. As seen in Fig. 3E, the final temperature and cooling rate drastically influence the complex shear modulus, while the effect of gap distance can be neglected.

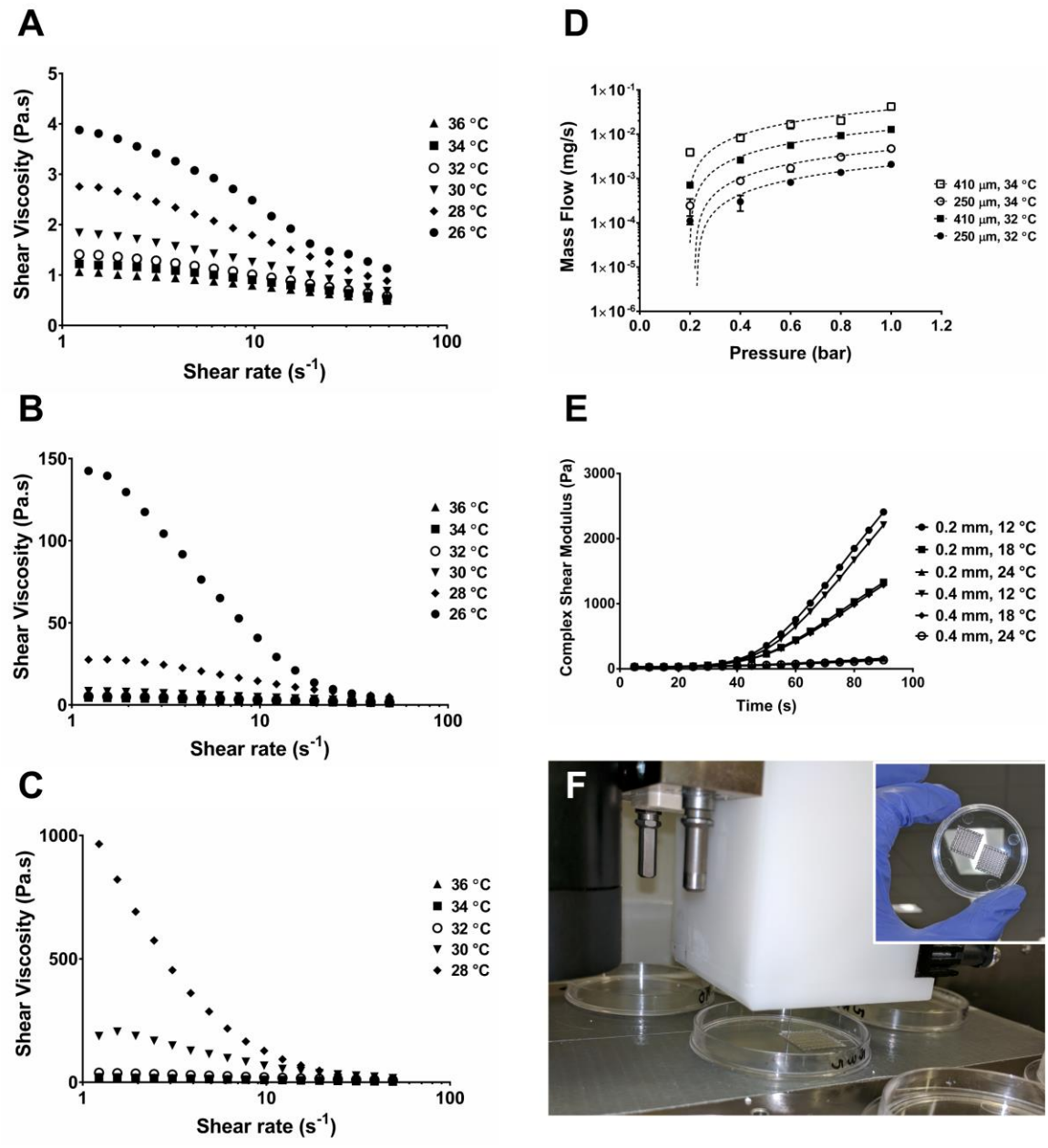

Figure 3. The shear viscosity of (A) G4E2H0.5, (B) G8E2H0.5, (C) G16E2H0.5 as a function of shear rate at different temperatures. (D) The mass flow rate of G8E2H0.5 as a function 3D-printer actual pressure, dispensing needle gauge and temperature. (E) The complex shear modulus of G8E2H0.5 as a function of time, gap distance, final temperature and cooling rate when the formulation is cooled between the rheometer parallel plates; the initial temperature was 32 °C and the material was cooled down to 12, 18 or 24 °C with a cooling rate of 10, 8 or 4 °C/min, respectively. (F) The printing procedure on petri-dishes and the obtained 3D-printed membranes.

The minor effect of surface area to volume ratio in the range examined can also be explained by heat transfer equations. As an example, two-dimensional heat conduction equation can be written as:

$$q = kS\Delta T \qquad \text{Eq. 2}$$

where q is the heat flow rate, k is the thermal conductivity, S is the shape factor and ΔT is the temperature difference. For an isothermal cylinder of radius "r" placed in semi-infinite medium, like the dispending needle placed in air, the shape factor is given as [50]:

$$S = \frac{2\pi L}{\ln\frac{2L}{r}}; \quad L \gg r \qquad \text{Eq. 3}$$

where L in the length of the cylinder/needle. The variation of the shape factor by even doubling the radius/diameter while keeping the length constant will be very small:

$$S_r = \frac{2\pi L}{\ln\frac{2L}{r}}; \quad S_{2r} = \frac{2\pi L}{\ln\frac{2L}{2r}} = \frac{2\pi L}{\ln\frac{L}{r}} \rightarrow \frac{S_{2r}}{S_r} = \frac{\ln\frac{2L}{r}}{\ln\frac{L}{r}} = 1 + \frac{\ln 2}{\ln\frac{L}{r}}; \quad \ln\frac{L}{r} \gg \ln 2$$

Considering ln (L/r) >> ln 2, the sensitivity of the shape factor to the variation of the radius is trivial. When the final temperature was set very close to room temperature (i.e. 24 °C), no significant increase in complex shear modulus was observed over time, suggesting the possibility of printing without confronting the needle obstruction. Reaching 12 °C with a high cooling rate resulted in a rapid rise of the complex modulus, which is in favor of shape fidelity. One may suggest to further reduce the platform temperature to achieve better shape fidelity. Such an assumption can be challenged by taking into account the fact that the platform temperature affects the dispensing needle temperature throughout the printing cycle and might drop it below the gelation temperature of the ink. Reflecting all the mentioned challenges, the parameters reported in the "methods" section were used to print the membranes.

3.2. Morphology, Line and Surface Roughness

Fig. 4 shows the surface morphology and characteristics of the printed membrane in both dehydrated and hydrated states. The roughness of the membrane surface was found to be in the micrometric range. The membranes had an average pore size of 286 and 374 μm in dehydrated and hydrated states, respectively. Hydration of the samples led to increased roughness (R_a and S_a) and pore size simply because of the swelling. Substrate topography at the micro- and nanoscale has been reported to impact cell attachment behavior [51]. Micrometer-scale surface roughness improves the cell attachment compared to smooth surfaces [52, 53]. It has been suggested that cells tend to maximize the contact area with the surface probably to establish a robust anchorage [51, 54]. The layout of the topographic details might then induce a specific cell alignment as a result [51].

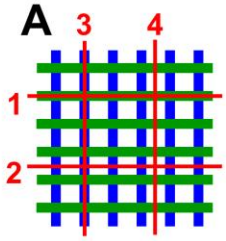

Sample	Line Roughness R_a (μm)				Strand Surface Roughness S_a (μm)	Film Surface Roughness S_a (μm)	Pore Size (μm)
	Direction 1	Direction 2	Direction 3	Direction 4			
Dehydrated	2.35 ± 0.09	9.10 ± 0.44	4.09 ± 0.28	10.17 ± 0.41	0.87 ± 0.29	7.43 ± 1.54	286 ± 40
Hydrated	9.16 ± 3.41	19.62 ± 3.54	13.49 ± 0.96	21.13 ± 1.42	1.94 ± 0.45	20.90 ± 1.44	374 ± 59

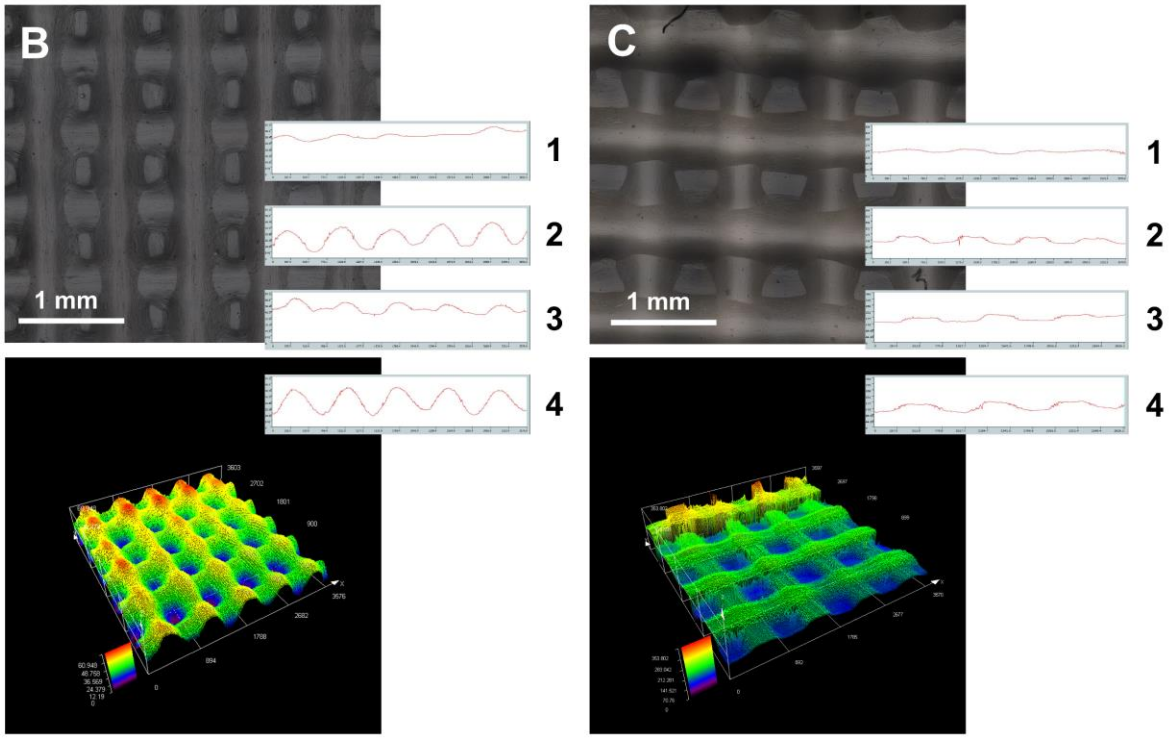

Figure 4. (A) Line roughness of the printed membrane measured in 4 different directions, surface roughness of the strands and the whole membrane and the average pore size in both dehydrated and hydrated states along with the morphology and height profile of the surface of the membrane as well as the histograms in all the specified directions for both (B) dehydrated and (C) hydrated states were obtained using laser microscopy.

3.3. In-Vitro Cell Attachment and Proliferation Assays

The results of the in-vitro cell viability and proliferation study indicate good biocompatibility. Absorbance values increased from 24 to 72 h and showed values close to the control group (tissue culture plate) (Figure 5). Additionally, SEM images of the membrane surface were obtained 48 h after cultivation. The images showed adhesion of corneal epithelial cells on the membrane surface. The cells kept their normal morphology and malformed cells were not observed. Moreover, signs of degradation were visible. The latter could be a culprit of the observed low count of cells on the membrane surface, since the cells could have migrated to subsurface regions through the intrinsic porous texture and porosity caused by degradation.

It should be noted that while it would be ideal to use conjunctival epithelial cells to conduct in vitro tests, a wide range of cell types have been suggested for assessing the efficacy of fabricated scaffolds for ocular surface/conjunctival reconstruction [55-62].

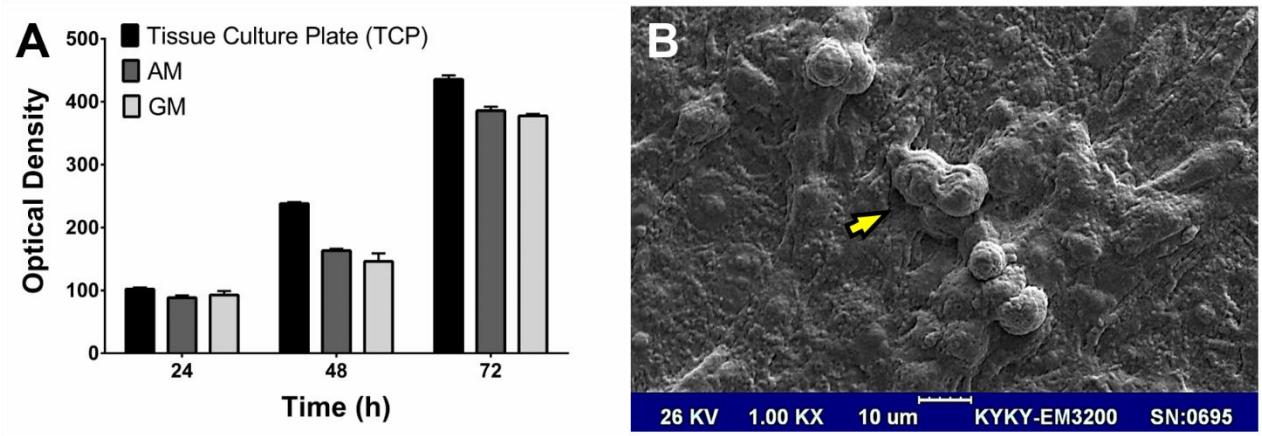

Figure 5. In vitro study of the samples. (A) MTT test absorption values at 24, 48 and 72 h. (B) SEM image illustrating partial gelatin-based membrane degradation and epithelial cell adhesion to the surface, 48 h after cultivation.

3.4. Mechanical Properties, Suturability and Assessment of Surgical Handling of the Membranes

The young's modulus, ultimate strength and suture retention strength of the gelatin-based membranes were found to be 170.2 ± 36.1 kPa, 95.4 ± 10.1 kPa and 20.4 ± 2.03 g, respectively (see supplementary information Fig. S3).

The pre-operative assessment showed that gelatin-based membranes were suturable, easy to manipulate with surgical forceps and had favorable rigidity. Surgical handling of the gelatin-based membrane appeared to be simpler in terms of cutting ease and placement in the defect (i.e. the membranes did not fold as much as AM did and upside-down placements were easily recognizable). These attributes made suturing easier with gelatin-based membranes (see supplementary videos-suturability). Also, the gelatin-based membranes showed a faster and stronger response to fibrin glue.

In addition to the ease of surgical handling, the gelatin-based membrane studied in this investigation had transparency and (potentially) geometrical conformity. The gelatin-based membranes can be fabricated in any shape (conforming to a given forniceal area shape), leveraging inherent capability of 3D printing in making complex geometries.

3.5. In-Vivo Conjunctival Tissue Reconstruction and Clinical Outcomes

Defects were artificially induced in supralateral bulbar conjunctivae of eighteen eyes using the method detailed in section 2.7. The final defect size had an average diameter of ~9 -10 mm due to retraction of adjacent Tenon. Two eyes (from two different rabbits, one left eye and one right eye) served as the control group and were left untreated. The remaining sixteen eyes (from eight different rabbits) were grafted with either AM or gelatin-based membranes. The number of left eyes grafted with AM was equal to the number of left eyes grafted with gelatin-based membranes. The right eyes had the same count of AM grafts and gelatin-based membranes as well.

3.5.1. Day 12 after surgery (2nd week)

Table 2 captures clinical outcomes for the second week. On day 12 after surgery, the mean defect diameter was 8.6 ± 1.8 mm (3-10 mm), 5.8 ± 1.7 mm (3-10 mm) and 0.0 mm for the gelatin-based membrane, AM and ungrafted eyes, respectively. No significant difference was observed between AM and the gelatin-based membrane groups ($p = 0.42$), while they were both significantly different from the control group ($p < 0.01$). Ungrafted wounds were completely epithelialized. Seven out of eight eyes grafted with AM showed epithelialization and vascularization at the edges of the

wound, while one eye had no epithelialization. In the gelatin-based membrane grafted group, two eyes showed epithelialization and vascularization at the wound edges, and six eyes showed no signs of epithelialization. Both eyes in the control group were completely epithelialized. The mean inflammatory response score showed a significant difference between groups ($p < 0.01$), but AM and gelatin-based membrane were not significantly different. The mean score was 0, 2.25 ± 0.48 (range 0-4) and 2.87 ± 0.24 for the control group, eyes grafted with the gelatin-based membranes and AM, respectively. Seven of the eyes in the AM group showed severe inflammation, while only three eyes showed severe inflammation in the gelatin-based membrane group (Table 2). Wounds grafted with either AM or the gelatin-based membrane showed infiltration with white debris that was confirmed to be composed of acute inflammatory cells in pathology and negative for microbial contamination. The AM-grafted eyes were more strongly infiltrated. The gelatin-based membrane and AM were partially degraded at day 12 after surgery at the peripheral edges, while remaining as a sheath in the defect site (70-80% of the initial defect). All the gelatin-based membranes had maintained their porous structure and showed slight whitening at day twelve. The covering conjunctivae did not show any gross remodeling and scar tissue formation in the control and both study groups except for one rabbit in the AM group, which showed moderate remodeling and contracture in the conjunctivae.

3.5.2. Day 19 after surgery (3rd week)

Table 3 captures clinical outcomes for the third week. On day 19 after the surgery, the mean defect diameter was 0.87 ± 1.45 mm (0-6 mm), 1.62 ± 2.45 mm (0-10 mm), and 0.0 mm for the gelatin-based membrane, AM and ungrafted eyes, respectively ($p = 0.73$). No significant difference was observed between the treated groups ($p = 0.87$). Six out of eight eyes grafted with AM showed complete epithelialization; one had a 3 mm defect, and one eye had no epithelialization. Complete epithelialization was also observed in six out of eight eyes implanted with the gelatin-based membrane, while two other eyes showed defects of 6 and 1 mm in size. The mean inflammation score was 0.0, 1.0 ± 0.9 (range 0-3) and 1.75 ± 0.88 (range 0-3) for the control group, and eyes grafted with the gelatin-based membranes and AM, respectively, which did not show any significant difference between neither all three groups ($p = 0.13$), nor the treated groups ($p = 0.27$). On day 19, three eyes in the AM group showed zero to mild inflammation and three eyes were still showing severe inflammation, while six out of eight eyes grafted with the gelatin-based membrane had zero to mild inflammation and two eyes had severe inflammation (Table 3). In the gelatin-based membrane group, inflammation was mainly seen in the surrounding host conjunctivae. Wounds grafted either with AM or the gelatin-based membrane still showed infiltration with white debris that was again confirmed

to be composed of acute inflammatory cells in pathology; microbial tests were again negative. However, AM-grafted eyes were still more strongly infiltrated and the control group showed no inflammatory response. The implanted gelatin-based membrane and AM could not be completely identified in 5 and 6 eyes in each group, respectively, and only 10-20% of the original grafts could be seen in the remaining eyes of both groups. Covering conjunctivae showed gross remodeling and scar tissue formation in both control eyes and in two AM grafted eyes but not in any of the gelatin-based membrane grafted eyes.

3.5.3. Day 28 (4th week)

Table 4 captures clinical outcomes for the fourth week. On day 28 after the surgery, all grafted and ungrafted wounds had completely epithelialized. The mean inflammatory response score showed a significant difference between all groups ($p < 0.01$) and between the treated groups ($p < 0.01$). The mean score was 0.0, 0.37 ± 0.35 (range 0-1), and 1.5 ± 0.63 (range 0-3) for the control group, eyes grafted with the gelatin-based membranes and AM, respectively. Wounds grafted either with AM or the gelatin-based membrane were still showing infiltration with white debris that was again confirmed to be composed of acute inflammatory cells in pathology and negative for microbial tests. The AM-grafted eyes were still more strongly infiltrated. The gelatin-based membrane and AM were not totally visible under the completely epithelialized surface except in two eyes in the gelatin-based membrane group, wherein the membranes were visible as sub-conjunctival prominences without significant inflammation of the adjacent conjunctivae. The covering conjunctivae showed gross remodeling and scar tissue formation in both of the control eyes, in three of the eight gelatin-based membrane grafted eyes and in six of the eight AM grafted eyes (Figure 6).

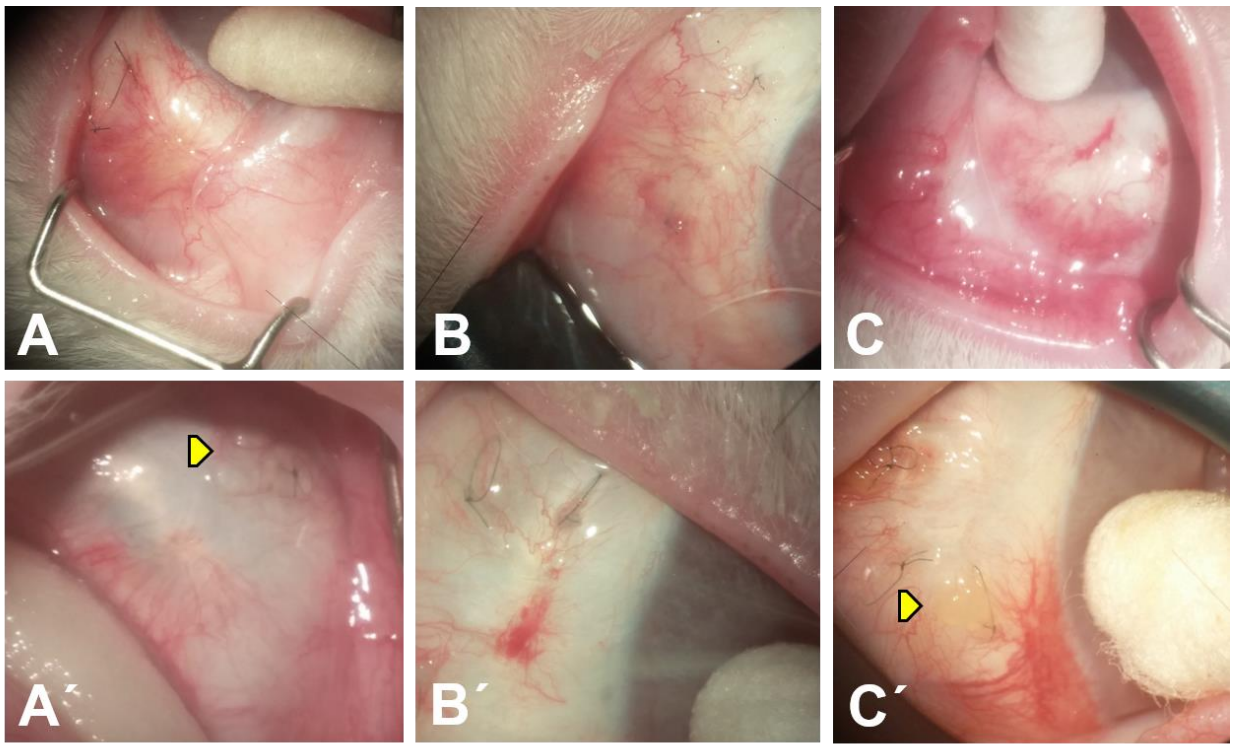

Figure 6. Clinical observation at day 28. (A-C) AM transplanted eyes. Gross conjunctival remodeling and inflammation can be observed. Inflammation is more abundant at the wound edges. (A & B) Non-degraded AM was observed in eyes showing yellowish discoloration under the repaired conjunctivae. (A′-C′) Gelatin-based membrane grafted eyes. Less inflammation and conjunctival remodeling was observed compared to AM grafted eyes. (A′) Remnant membrane pieces can be seen under the conjunctiva (arrowhead) with no significant adjacent inflammation. (C′) White debris clinging onto a suture in a gelatin-based membrane grafted eye. The trend of clinical observations is shown in Figure 7.

Epithelialization rate of conjunctival defects in rabbits has been reported to be approximately 0.2-0.3 mm^2/hr [63]. Given that and considering the average defect size of ~ 63.5-78.5 mm^2 in our study, the epithelization should be completed in ~ 13-16 days. Noting that complete epithelialization was observed by the second week for both eyes in the control group, our planned time of ~ 13-16 days was validated and consistent with prior observations reporting the complete epithelialization between the first and second week in untreated eyes [8, 10]. Early signs of epithelialization were observed in the second week in 25% of the gelatin-based membrane-grafted eyes, compared to 75% in the AM-grafted cases and the mean defect size was approximately 3 mm smaller in the AM-grafted group. However, this difference did not appear to be statistically significant, which could be due to

the small sample size (eight rabbits per group). This difference began to subside and reached about 1 mm (less in gelatin-based membrane grafted eyes) at the end of the third week, wherein 75% of both grafted wounds showed complete epithelialization. Maximum reduction in the defect size was observed during the third week for both grafted groups. Hence, it would be accurate to say that epithelialization began somewhere between the second and third weeks for the gelatin-based membrane grafted group and approximately a week earlier for the AM grafted eyes. Taking into account the degradation profile of gelatin-based membranes (see supplementary information, Figure S4), it would be fair to conclude that the gelatin-based membrane met the time requirements of the conjunctival epithelial repair.

In terms of inflammation, the gelatin-based membrane grafted group consistently showed milder degrees of clinically observed inflammation throughout the healing period compared to AM grafted eyes. A stark contrast in inflammation degree existed between the gelatin-based membrane and AM-grafted groups at week one. Severe inflammation was seen in 87.5% (7 out of 8 eyes) of AM grafted eyes compared to 37.5% (3 out of 8 eyes) of the gelatin-based membrane implanted eyes. This difference subsided at week three, but again became significant at the end of the fourth week, wherein no moderate or severe inflammation remained in the gelatin-based membrane-grafted group while three eyes were still showing moderate degrees of inflammation in the AM group. This observation suggests a plausible likelihood for long-term inflammation in AM-grafted eyes, for which possible mechanisms will be discussed in section 3.6. Early inflammatory responses could also be attributed to a reaction towards the preparation/preservation solutions and antibiotics, however, this factor was attempted to be limited by washing AM in balanced saline solution before transplantation. The trend of clinical observations is shown in Figure 7.

Additionally, gross conjunctival remodeling was seen in both eyes of the control group, which is in agreement with other studies showing increased scar formation in conjunctivae when left untreated [8, 9, 12]. However, fornix foreshortening was an indicator of scar tissue formation in the latter studies, with one having the defect involving the forniceal area [12]. We did not use fornix foreshortening for scar tissue formation evaluation, as the defect was not distended towards the fornix, and anchoring sutures were not applied in the forniceal area. Mild to moderate gross remodeling was seen in 75% of AM-grafted eyes compared to 25% in the gelatin-based membrane grafted group on the fourth week, which can be attributed to prolonged inflammation of the AM-grafted eyes (details in section 3.6).

Table 2: Clinical Outcomes for 2nd Week

	Inflammation Histogram			*Defect Size*			*Tissue Contraction*		
	Bare	*Gelatin-based Membrane*	*AM*	*Bare*	*Gelatin-based Membrane*	*AM*	*Bare*	*Gelatin-based Membrane*	*AM*
Rabbit 1		2.0	3.0		3.0	3.0		*None*	*Moderate*
Rabbit 2		3.0	3.0		10.0	10.0		*None*	*None*
Rabbit 3		2.0	3.0		10.0	3.0		*None*	*None*
Rabbit 4		2.0	3.0		10.0	8.0		*None*	*None*
Rabbit 5		1.0	3.0		10.0	6.0		*None*	*None*
Rabbit 6		3.0	2.0		10.0	4.0		*None*	*None*
Rabbit 7		3.0	3.0		10.0	5.0		*None*	*None*
Rabbit 8		2.0	3.0		6.0	8.0		*None*	*None*
Rabbit 9	*0*			0			*None*		
Rabbit 10	*0*			0			*None*		

Table 3: Clinical Outcomes for 3rd Week

	Inflammation Histogram			*Defect Size*			*Tissue Contraction*		
	Bare	*Gelatin-based Membrane*	*AM*	*Bare*	*Gelatin-based Membrane*	*AM*	*Bare*	*Gelatin-based Membrane*	*AM*
Rabbit 1		*0.0*	*2.0*		*0.0*	*0.0*		*None*	*Moderate*
Rabbit2		*1.0*	*2.0*		*6.0*	*10.0*		*None*	*None*
Rabbit 3		*0.0*	*0.0*		*0.0*	*0.0*		*None*	*None*
Rabbit 4		*1.0*	*1.0*		*0.0*	*3.0*		*None*	*None*
Rabbit 5		*0.0*	*3.0*		*0.0*	*0.0*		*None*	*None*
Rabbit 6		*3.0*	*0.0*		*0.0*	*0.0*		*None*	*None*
Rabbit 7		*3.0*	*3.0*		*1.0*	*0.0*		*None*	*Moderate*
Rabbit 8		*0.0*	*3.0*		*0.0*	*0.0*		*None*	*None*
Rabbit 9	*0*			*0*			*Mild*		
Rabbit 10	*0*			*0*			*Mild*		

Table 4: Clinical Outcomes for 4th Week

	Inflammation Histogram			*Defect Size*			*Tissue Contraction*		
	Bare	*Gelatin-based Membrane*	*AM*	*Bare*	*Gelatin-based Membrane*	*AM*	*Bare*	*Gelatin-based Membrane*	*AM*
Rabbit 1		*0*	*1*		*0*	*0*		*Moderate (Star Shaped Scar)*	*Moderate (Star Shaped Scar)*
Rabbit2		*0.0*	*1.0*		*0*	*0*		*Mild*	*Moderate*
Rabbit 3		*0.0*	*1.0*		*0*	*0*		*None*	*Mild*
Rabbit 4		*0.0*	*1.0*		*0*	*0*		*None*	*Mild*
Rabbit 5		*1.0*	*2.0*		*0*	*0*		*None*	*Moderate*
Rabbit 6		*1.0*	*2.0*		*0*	*0*		*None*	*None*
Rabbit 7		*1.0*	*0.0*		*0*	*0*		*None*	*None*
Rabbit 8		*0.0*	*2.0*		*0*	*0*		*Mild*	*Moderate*
Rabbit 9	*0*			*0*			*Mild*		
Rabbit 10	*0*			*0*			*Mild*		

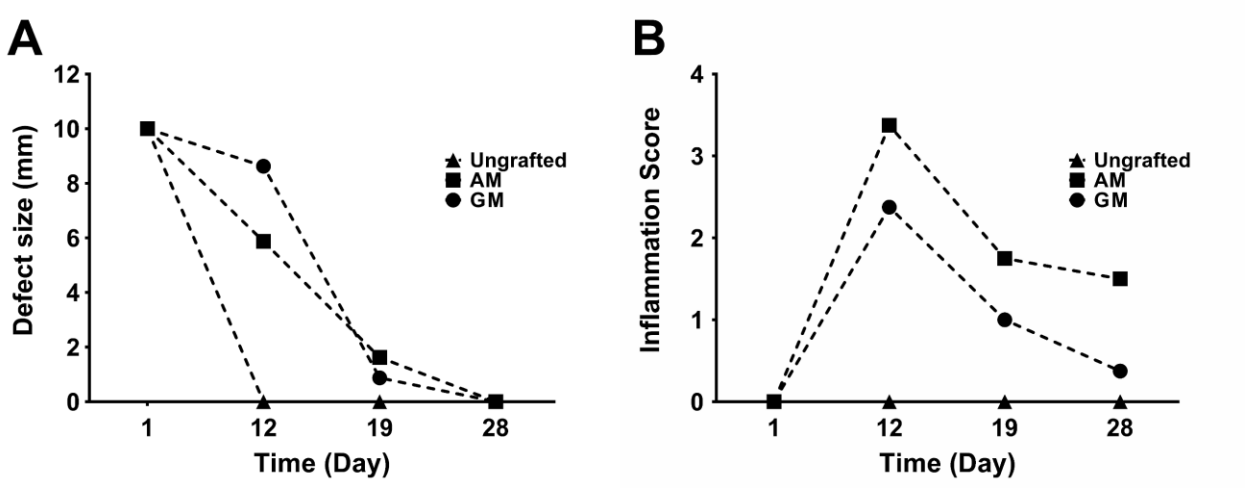

Figure 7. Clinical Observations: (A) the defect size and (B) the inflammation score at 1st, 12th, 19th and 28th days post-implantation.

3.6. Histological Assessment of Repaired Conjunctival Tissue

3.6.1. H&E staining

H&E staining was done at the end of week 4 to assess the characteristics of the repaired conjunctivae. Complete epithelialization of the defect was seen in all groups (continuous). The repaired epithelium consisted of 3-5 layers of epithelial cells in eight of the gelatin-based membrane grafted and seven of the AM grafted eyes. All eyes grafted, whether with gelatin-based membrane or AM, showed normal cuboidal basal cells and flattening of the epithelial cells towards the surface. However, less than 3 layers of epithelium were observed in both control eyes with none showing flattening of the epithelial cells towards the surface and normal cuboidal basal cells (Figure 8). Squamous metaplasia was seen in two of the eyes grafted with AM. Goblet cells had normal morphology in all groups (Table 5).

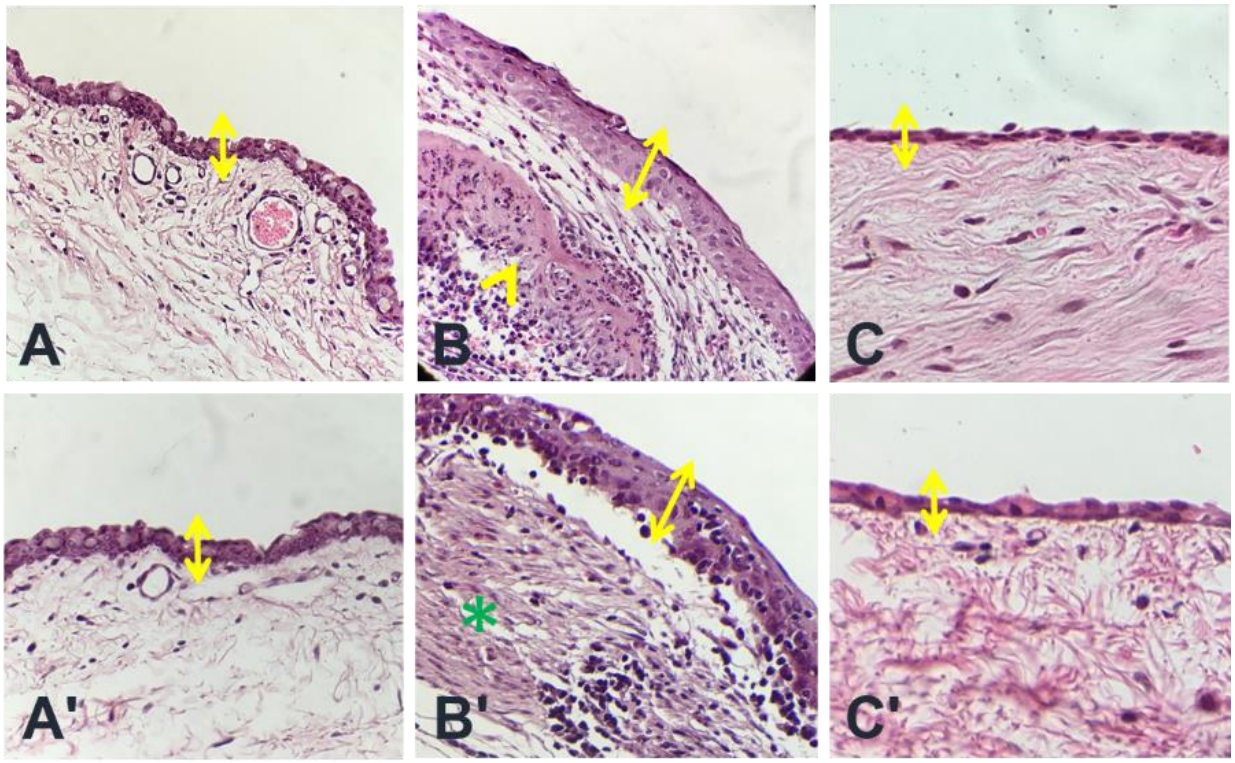

Figure 8. H&E staining; (A & A′) gelatin-based membrane grafted eyes: 3-5 layers of epithelial cells (yellow double arrow) are seen in the repaired epithelium with normal cellular morphology. (B & B′) Amniotic membrane grafted eyes: 3-5 layers of epithelial cells (yellow double arrow). (B) Squamous metaplasia of epithelium (large cells with increased nuclear to cytoplasmic ratio) and remnant AM can be seen in sub-epithelial stroma (yellow arrowhead) with adjacent inflammatory reaction. (B′) Severe inflammatory reaction in site of transplantation. (C & C′) Ungrafted eyes: thin epithelium with non-satisfactory flattening of epithelial cells, especially in C′.

The membranes showed complete degradation in six out of eight of gelatin-based membrane grafted eyes and membrane remnants were seen in three eyes, while only one eye in the AM group showed complete degradation and AM remnant was seen in seven out of eight eyes grafted with AM.

The host inflammatory response was compared in the three groups. All eyes implanted with the gelatin-based membranes had inflammatory scores of less than one; four eyes showed no inflammation and the remaining four showed a mild inflammatory response. Of the two eyes in the control group, one showed none, and one showed a mild inflammatory response. In contrast, all eyes in the AM grafted group showed inflammatory responses. The inflammatory response was severe in six eyes and moderate in two eyes ($p < 0.001$ between all three, as well as between the two treated groups). The inflammatory cells consisted of lymphocytes and plasma cells in all

groups. Mast cells were seen in the eyes of the AM grafted group. Histiocytes and giant cells, suggestive of granulomatous response, were present in seven out of the eight AM grafted eyes, while being present in only one of the gelatin-based membrane grafted eyes ($p < 0.001$ between all three as well as two treated groups) (Table 6). Figure 9 shows the host's inflammatory response towards the remaining membrane and AM.

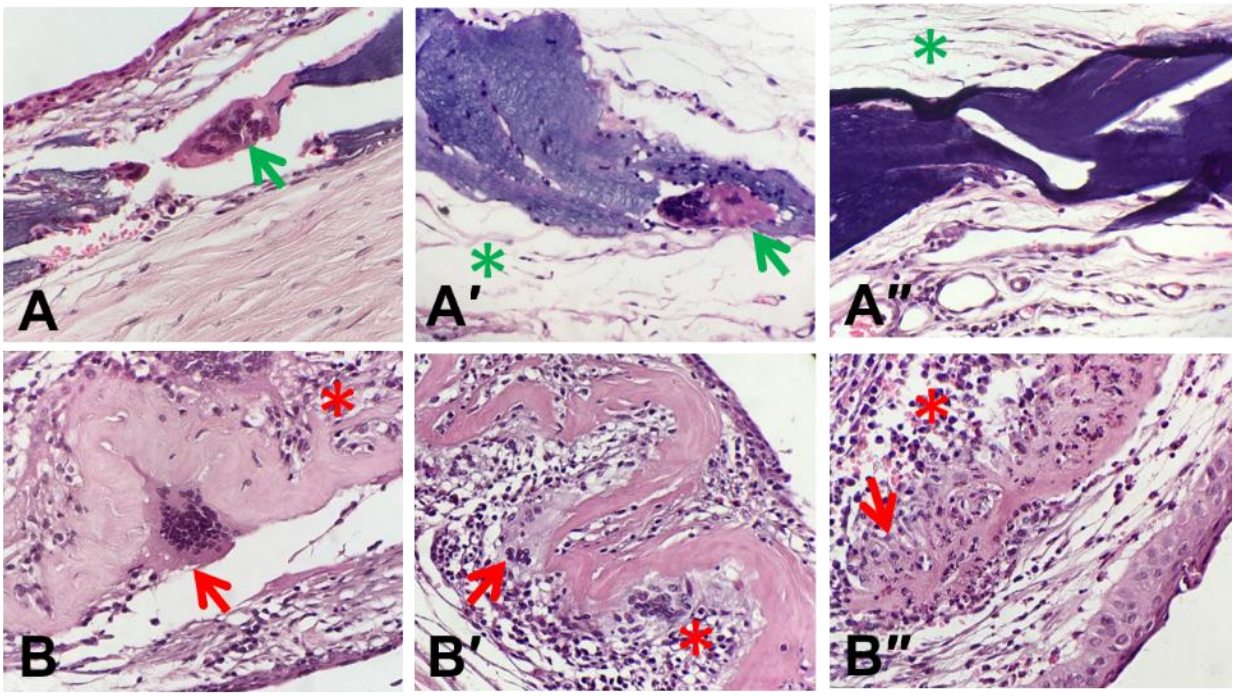

Figure 9. H&E staining; (A & A′ & A″) Macrophages (green arrow) are digesting the gelatin-based membrane without an adjacent significant inflammatory response (green asterisk). (B & B′ & B″) Multiple giant cells (red arrow) along with a severe inflammatory response (red asterisk) composed of monocyte, macrophage and mast cells are seen around the remaining AM.

3.6.2. PAS staining

PAS staining was performed to evaluate goblet cell density and compare it between the groups. Goblet cell counts per 100 cells were 2.50 ± 0.97, 10.87 ± 5.17 and 5.37 ± 2.68 in the control, the gelatin-based membrane and the AM grafted groups, respectively ($p = 0.13$ between all three groups and $p = 0.18$ between AM and gelatin-based membrane treated groups). Goblet cell counts of 10 and more were seen in five of the gelatin-based membrane grafted and two of the AM grafted eyes. No goblet cells were observed in eyes of the control group (Fisher's exact: $p = 0.42$ between all three groups, and $p = 0.41$ between AM and gelatin-based membrane treated groups) (Figure 10, table 5).

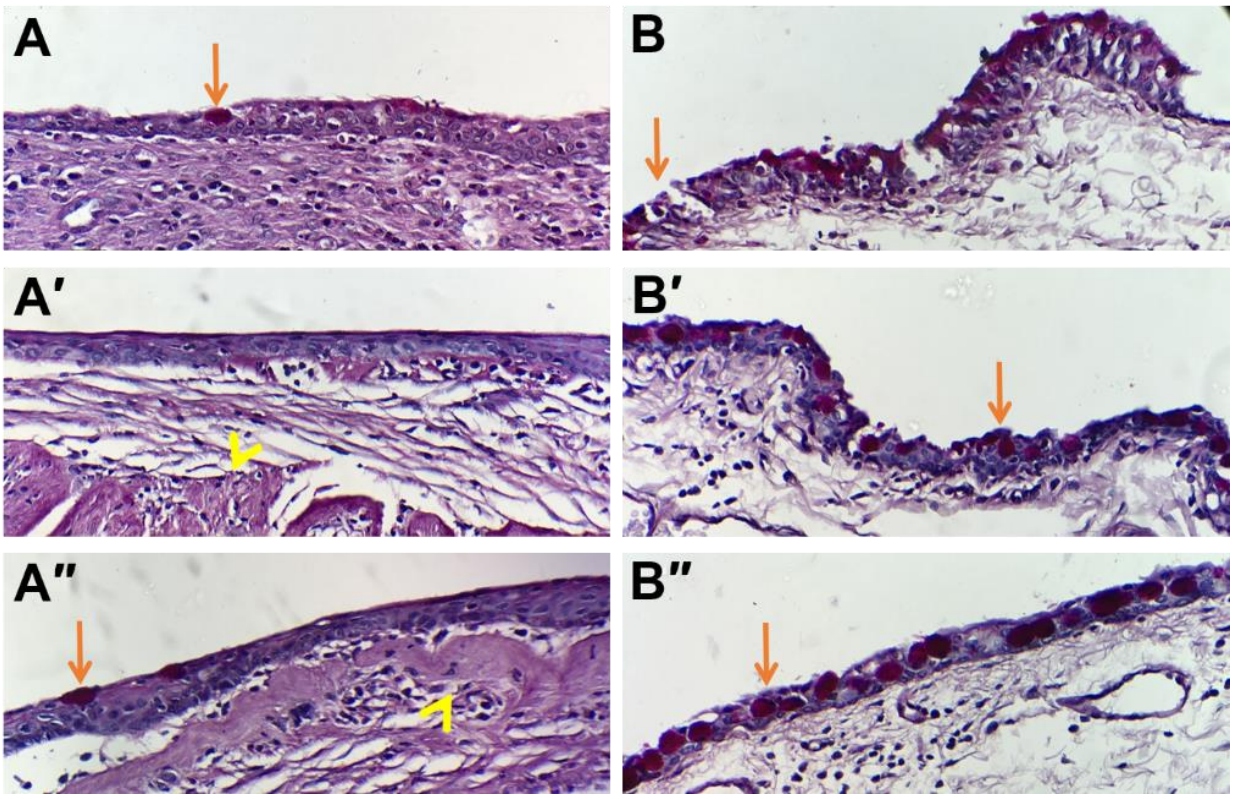

Figure 10. PAS staining: (A&A′&A″) Amniotic membrane grafted eyes: Less than 10 goblet cells (orange arrows) per 100 cells are seen along the repaired epithelium. Remnant amniotic membrane (yellow arrow head) is seen in the sub-epithelial area with adjacent inflammatory cells and fibrosis. (B&B′&B″) Gelatin-based membrane grafted eyes: 10 or more goblet cells per 100 cells are seen in the repaired epithelium. The sub-epithelial stoma shows no abundant inflammatory cell infiltration.

3.6.3. Masson trichrome staining

Masson trichrome staining was carried out to evaluate the details of the sub-epithelial regenerated stroma. Comparing collagen alignment between the groups showed that collagen fibrils were aligned irregularly and angled, forming a loose and spongy stroma resembling that of the normal conjunctivae in all (eight) gelatin-based membrane grafted eyes, while composing a dense matrix of parallel and packed collagen fibrils in AM grafted eyes. The latter was especially seen adjacent to AM remnants. The sub-epithelial stroma in both ungrafted eyes showed a dense and thick layer (approximately 3 times thicker that the layer in the AM group) of parallel and densely packed collagen fibers under the thin epithelium (Figure 10). The collagen alignment difference was significant ($p < 0.001$) between all three groups, as well as between the treated groups (Table 6).

3.6.4. Immunohistochemical staining for α-SMA

Immunohistochemical staining for α-SMA was carried out to evaluate and compare the presence of myofibroblasts (cells with contractile potentials) in the study groups. Smooth muscle cells of adjacent extraocular muscles and vascular pericytes are α-SMA-positive. α-SMA-positive cells, which had an elongated and fibroblast like morphology, were considered myofibroblasts (potentially contractile cells). Myofibroblasts were seen in four of the gelatin-based membrane grafted eyes, two contained many α-SMA-positive cells and two showed a moderate infiltration of cells into the stroma. The AM-grafted eyes staining outcome for the latter cell was positive in seven eyes, six of which showed severe infiltration and one showed moderate infiltration of cells in stromal tissue. α-SMA staining did not show any significant difference (p=0.25) between gelatin-based membrane and AM-grafted groups (Figure 11 and Table 6).

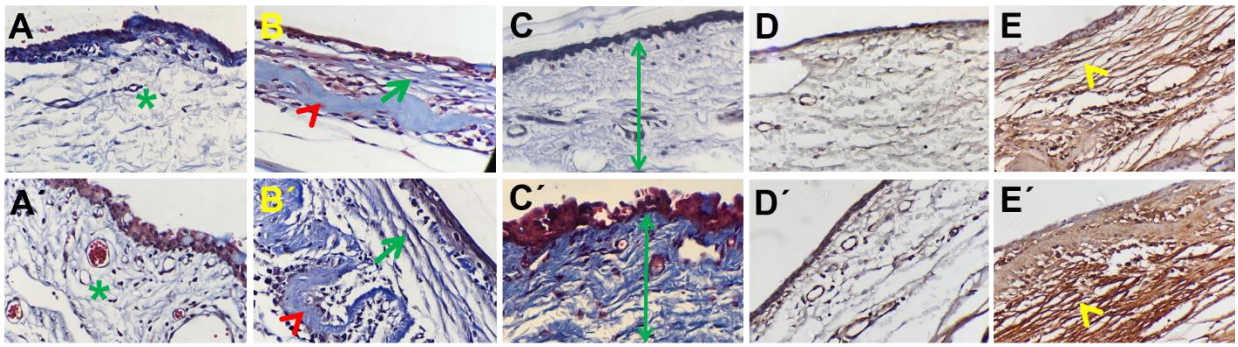

Figure 11. Masson trichrome staining and IHC for α-SMA: (A&A′) gelatin-based membrane grafted eyes showed random alignment of collagen fibers (green asterisk) while (B&B′) AM grafted eyes showed parallel deposition of collagen (green arrow) along the AM remnant (red arrow head). (C&C′) A thick layer of densely packed collagen fibers was seen in both ungrafted eyes. (D&D′) Gelatin-based membrane grafted eyes exhibited no α-SMA-positive cells while (E&E′) AM grafted eyes exhibited numerous elongated α-SMA-positive cells.

Table 5: Comparison of healed epithelium characteristics between gelatin-based membrane, AM and ungrafted eyes

Epithelium characteristics	*Bare*	*Gelatin-based Membrane*	*AM*	
				Fisher's exact test
Epithelial layers				
<3	*2*	*0*	*1*	*p = 0.02*
3-5	*0*	*8*	*7*	
>5	*0*	*0*	*0*	
Flattening				
Yes	*0*	*8*	*8*	*p = 0.007*
No	*2*	*0*	*0*	
Goblet count/100 cells				
	2.50 ± 0.97 (2-3)	*10.87 ± 5.17 (2-21)*	*5.37 ± 2.68 (2-12)*	*Kruskal wallis p = 0.13*

Table 6: Comparison of inflammation (severity and type) and characteristics of the healed stroma between gelatin-based membrane, AM and ungrafted eyes (for details about grading criteria, see supplementary information)

Inflammation	*Bare*	*Gelatin-based Membrane*	*AM*	
				Fisher's exact test
Inflammation				
None (0)	*1(50%)*	*4(50%)*	*0*	*p < 0.001*
Mild (1)	*0*	*4(50%)*	*0*	
Moderate (2)	*1(50%)*	*0*	*2(25%)*	
Severe (3)	*0*	*0*	*6(75%)*	
Granulomatous reaction	*1*	*1*	*7*	*p = 0.01*
Non-granulomatous reaction	*0*	*3*	*1*	
Collagen deposition				
Linear compact	*2*	*1partially*	*8*	*p < 0.001*
Irregular and loose	*2*	*8*	*0*	
α-SMA				
Negative	*NA**	*4*	*1*	*p = 0.25*
Positive	*NA*	*4*	*7*	

*Not assessed

4. Discussion

The gelatin-based membranes, in this study, offered ease of surgical handling, transparency and potentially geometrical conformity. Conformity is a particularly crucial factor in conjunctival reconstruction within the forniceal area, since placing anchoring sutures would be very difficult, if not impossible, if the membrane does not conform to the shape of the fornix. Conformity is of the utmost importance in diseases that cause forniceal shortening, like ocular burns and autoimmune diseases [13, 19, 64]. Transparency is an advantage in terms of better cosmetic results; materials such as poly(lactic-co-glycolic acid)(PLGA) and Collagen-Glycosaminoglycan (CG) are not transparent, and AM has been reported to result in a blunted conjunctival appearance and decreased clarity until complete degradation [32]. Surgical handling can influence the reconstruction process. As an example, conjunctival reconstruction using CG copolymer matrix scaffolds with 2 mm thickness can lead to unfavorable results due to an increased likelihood of step formation that can hinder epithelial cells migration [9].

Prior studies have reported the completion of epithelialization after two weeks when PGLA or CG copolymers were used [8, 9]. For vitrified collagen cases, it has been reported that epithelialization started in the first week and complete repair was observed in the fourth week [12]. Given these results, the response of the membranes studied in this investigation were comparable to that of other synthetic materials, albeit somewhat delayed compared to AM-grafted cases. Huang et al. has reported the time required for complete epithelialization to be two weeks in a rabbit model grafted with AM [10]. Interestingly, the degradation profile of the gelatin-based membranes is well-matched with the required time for epithelialization. The better quality of the resultant healed conjunctiva for the gelatin-based membrane grafted eyes ca be seen in histological examinations (details in section 3.6). The quality of the repaired epithelium seems to be more promising, in terms of stratification and goblet density, in the gelatin-based membrane implanted eyes, compared to currently used tissue engineered scaffolds. Eyes treated with the gelatin-based membrane showed 3-5 layers of stratification, while Zhou et al. reported decreased number of epithelial layers with a flattened epithelial cell morphology in rabbit eyes grafted with collagen virtrigel and eyes left ungrafted [12]. Lee et al. [8] and Hsu et al. [9] reported 2-3 layers of epithelial cells in modified PLGA and CG copolymer grafted rabbit eyes, respectively.

Goblet cell density was found to be approximately 10 cells per every 100 cells for the gelatin-based membrane grafted eyes, which is the highest density for goblet cells reported between recently evaluated non-seeded bioengineered materials. CG copolymer scaffolds and acellular vitrified

collagen material have shown to have very low to absent concentration of goblet cells in the repaired conjunctivae [9, 12]. In the latter study, vitrified collagen seeded with conjunctival epithelial cells obtained 23% goblet density compared to 30% in the normal conjunctivae [12]. Goblet cell density has not been reported in the study on the PLGA [8]. However, NormalGEN, derived from bovine pericardium for conjunctival reconstruction, has been reported to bring about a goblet cell density similar to native conjunctivae, but the epithelium is thin and contains fewer layers. The results with regard to goblet cell density were more promising in the gelatin-based membrane grafted eyes compared to AM grafted eyes. The mean goblet cell count was approximately twice as much in the gelatin-based membrane grafted eyes compared to the AM grafted eyes, with 50% of the eyes having counts higher than 10 per total 100 cells, compared to 25% having more than 10 per total 100 cells in the AM grafted eyes. However, this difference was not significant, probably due to the small sample size. The relatively more severe and prolonged inflammation in AM grafted eyes may lead to lower goblet cell count in this group. Evaluation of specific mucin secretions, such as MUC5AC and MUC 2 is recommended for future studies, as it can provide additional comparative information on the differences in mucinous secretion regulation on differently repaired conjunctival surfaces.

Additionally, the results of epithelialization for the gelatin-based membrane were comparable to the most widely used substitute (i.e. AM). Both groups showed approximately equal layers of epithelial stratification (3-5), normal epithelial morphology and flattening towards the surface in histological examination.

The results here are consistent with other studies, showing that AM can promote epithelialization [18, 19, 21, 27]. Two eyes in the AM grafted groups showed epithelial metaplasia, which did not seem to be a consequence of the inflammation seen in the AM group as both eyes had moderate inflammation with a mean goblet cell count of 10. Metaplasia after AM transplantation was also observed in five out of nine eyes in a study using AM for conjunctival reconstruction after symblepharon removal in OCP patients (by impression cytology) [13]; more studies need to be carried out on this topic.

Studies supporting goblet cell repopulation on AM have been mostly conducted through cultivation of conjunctival epithelial cells on AM. Additionally, most of the studies have not reported the percentage of goblet cells [34, 65, 66]. Three in vivo studies on rabbits have also reported goblet cell repopulation after implantation of cryopreserved AM for conjunctival reconstruction, but none have reported the number of cells [10, 65, 67].

In a study conducted on human conjunctival repair using AM after scar tissue and symblepharon removal, restoration of goblet cells was reported in 6 out of 9 eyes (66.7%) in the 4th week of examination. However, only 4 eyes (44.4%) had the normal conjunctival epithelium, with goblet cells restored, in the 28th week of examination. The results were based on impression cytology and no histological data was given. The time to complete epithelialization was similar to our study, i.e. 3 weeks [68]. In another study, goblet cell density was reported to be 10 times as much in patients receiving AM after iatrogenic conjunctival removal compared to a control group. Again, the data was based on impression cytology and no histological data was given [66].

Our results suggest that both gelatin-based membrane and AM can provide a favorable base for epithelial cell migration and proliferation. The short delay in epithelialization in the gelatin-based membrane group is not clinically important, as the repaired epithelium showed similar quality in both groups eventually. The outcome for ungrafted eyes (i.e. thin epithelium; low stratification) and reduced goblet cell density were consistent with other studies [9, 10, 12].

The major difference between the results of the eyes grafted with gelatin-based membrane versus eyes grafted with AM was in the host's inflammatory response seen in histological sections of the graft site. As shown in the results, no inflammatory cells were seen in 50% (4 eyes) of the eyes treated with gelatin-based membranes, and the remaining eyes showed only a mild response that was mostly non-granulomatous. On the other hand, all eight eyes treated with AM continued to show an inflammatory response up to the 28th day, with seven out of eight (87.5%) being granulomatous.

Cryopreserved amniotic membrane has been shown to have anti-inflammatory and, consequently, anti-scarring properties. The anti-inflammatory mechanism of AM is not fully understood yet. In-vitro studies suggest that AM can inhibit expression of pro-inflammatory cytokines such as interleukin (IL) 1a, IL-1b [69] and IL-8 [70]. It contains immunomodulatory substrates, such as heavy chain (HC)-hyaluronan (HA)/pentraxin 3 (PTX3) in its matrix [21]. Anti-scarring effects have been attributed to AM's ability to reduce expression of TGF β-1, β-2, β-3 and TGF receptor, and consequent inhibition of conjunctival fibroblast proliferation [71].

The current study, however, suggests active presence of lymphocytes and lymphoplasma cells around the undegraded AM after 28 days of transplantation, based on histological sections.

Histologically confirmed inflammation around the AM has also been reported in a similar study on AM transplantation in rabbits for conjunctival reconstruction, where an increase in severity of monocyte infiltration up until day 28 and eventual decrease in day 58 after transplantation were observed [10]. A similar observation on the 36th and 60th day after filtering surgery has been reported by two other studies, where cryopreserved and dry human AM were used, respectively [28, 29]. In contrast, the images provided in a study on rhesus monkeys using AM for conjunctival reconstruction did not display any significant inflammatory response two weeks after transplantation [30].

It has been suggested that AM traps and then induces apoptosis in inflammatory cells in damaged ocular surfaces [21, 72]. Considering AM's ability to trap inflammatory cells, prolonged presence of AM in donor tissues, reflecting unpredictable degradation rate, may be the reason for the longstanding mononuclear inflammatory response seen in this study and others [10, 28, 29], as cells are seen to be just surrounding the AM, not distributed in the donor stroma. The remnant has been reported to remain 3-10 weeks after cryopreserved AM transplantation in pemphigoid patient's eyes [13] and 9 weeks after transplantation of dry and cryopreserved AM in rabbit eyes [28, 29]. On the other hand, the ability to induce apoptosis in inflammatory cells and subsequently reduce inflammation, or other anti-inflammatory mechanisms of AM [20, 70, 72, 73], may compensate for certain types of inflammation to certain degrees. However, it becomes less effective when the inflammation is severe [1, 19, 21, 26]. Considering the low inherent immunogenicity of AM and acellularity of the remnants of AM in the histological sections weakens the assumption of xenograft rejection, whereby AM is surrounded by mononuclear cells [28, 29, 74]. Evaluation of the statistics of different inflammatory cells using immunohistochemistry markers, provision of detailed information about their exact composition [75], and the assessment of tear inflammatory factors during the repair process may also be beneficial in classifying and characterizing the reactive/inflammatory processes and conducting further future studies.

Another important group of cells found in this study were histiocytes and giant cells, the hallmarks of chronic inflammation, revealing foreign body reaction towards AM. Such reactions were not seen in the gelatin-based membrane group. Granulomatous reaction towards AM has been observed by others at day 14 after human AM transplantation in rabbits [28]. Granulomatous tissue was observed in the vicinity of suture remnants in all sections. The least possible number of sutures was used in this study to prevent suture reactions from being confounded with the inflammation data. It is also important to note that the strong and rapid response of gelatin-based membranes to fibrin glue thus serves as another advantage of such biomaterials. Less favorable outcomes using

sutures have been reported in clinical studies [76], as sutures themselves induce foreign body reaction.

Both gelatin-based membrane and AM grafted eyes showed less parallel alignment of collagen compared to the control group. The application of porous scaffolds has previously been reported to decrease scar formation. More randomly aligned collagen deposition compared to ungrafted wounds has been suggested as the possible mechanism [8-10, 12]. The obtained results are consistent with the anti-scaring effects reported for AM [71, 77, 78]. However, there was a significant difference between the AM and gelatin-based membrane grafted groups, as near all eyes transplanted with the gelatin-based membrane showed random alignment similar to normal conjunctiva and fewer eyes were positive for ∝-SMA. In contrast, AM transplanted eyes revealed a much thinner layer of collagen deposition compared to control eyes. In addition to parallel and packed deposition of collagen in the vicinity of AM, positive ∝-SMA results in all eyes containing non-degraded AM (equal to 87.5%; i.e. 7 out of 8 eyes) were seen. Observed sub-conjunctival fibrosis (aligned and compact collagen deposition) can mainly be attributed to the prolonged presence of inflammation near the AM [20, 28]. A similar study on AM transplantation in conjunctival defects on rabbits showed that even though it was decreasing by the fourth week following transplantation, the fibroblast count increased on day 58 [10]. It may suggest the reduction of anti-inflammatory or anti-scaring effects of AM over time. Inefficacy or reduction of such effects have been previously observed specifically when the host's baseline inflammation is poorly controlled, such as with ocular cicatricial pemphigoid [13, 19, 76].

The gelatin-based membrane in this study led to similar quality of the healed epithelium in terms of cell morphology, cell layers and alignment of collagen compared to the widely used AM. Similar epithelialization time but significantly lower levels of clinical inflammation in gelatin-based membrane group is a key advantage of using the printed membrane over the AM. The observed similarities and differences can be somewhat explained by looking into the similarities and differences in composition, degradation profile and surface topography. Collagen IV is the major component of the basal lamina of AM used for ocular surface reconstruction [79] while gelatin is the main element in the printed membranes. Gelatin, as a collagen driven protein, offers comparable bioactivity due to similar functional groups and chemical composition while eliminating immunogenicity due to its denatured structure. Gelatin-based membranes have near complete degradation by day 28 with no histiocytic reaction in the vicinity of the remaining material suggesting biocompatibility and good tolerability by the host's immune cells. In contrast, long-lasting remnants of AM can cause prolonged presence of inflammation and sub-conjunctival fibrosis. Surface

roughness outlined by 3D-printing may also affect cell attachment and tissue reconstruction and can be further investigated in future studies.

5. Conclusions

In the current study, a 3D-printed membrane was fabricated using gelatin, elastin and sodium hyaluronate blend and was compared to amniotic membrane (AM) for conjunctival reconstruction. In-vivo experiments were conducted on induced conjunctival defects in rabbits. Clinical observations and histological examination suggested that the gelatin-based membranes is a promising synthetic substitute for AM in conjunctival reconstruction due to the following findings: 1) acceptable surgical handling, 2) favorable cell adhesion and proliferation on the membranes, 3) providing a promising stroma for expansion and proliferation of epithelial cells with normal morphology, 4) favorable epithelial cell morphology and acceptable goblet cell density of the repaired epithelium, 5) deterring unfavorable host inflammatory reactions and 6) complete degradation by day 28.

6. Acknowledgements

This work was carried out with support from China Regenerative Medicine International Limited (CRMI). The stem cell preparation unit (SPU) at Farabi Hospital, particularly Mr. Zarrabi, Mrs. Aghajanpour and Mr. Mohammadnia were very instrumental in conducting the in-vitro and in-vivo tests.

7. Data Availability

The raw/processed data required to reproduce these findings cannot be shared at this time as the data also forms part of an ongoing study.

8. References

[1] Meller D, Pires RTF, Mack RJS, Figueiredo F, Heiligenhaus A, Park WC, et al. Amniotic membrane transplantation for acute chemical or thermal burns. Ophthalmology.107:980-9.
[2] Gregory DG. The ophthalmologic management of acute Stevens-Johnson syndrome. Ocul Surf. 2008;6:87-95.
[3] Stefano Barabino M, 1 Maurizio Rolando, MD,1 Giorgio Bentivoglio, MD,2 Cristina Mingari, MD,3 Sabrina Zanardi, PhD,4 Rosa Bellomo, PhD,5 Giovanni Calabria, MD,PhD. Role of Amniotic Membrane Transplantation for Conjunctival Reconstruction in Ocular-Cicatricial Pemphigoid. ophthalmology. 2003:110:474–80.
[4] Li M, Zhu M, Yu Y, Gong L, Zhao N, Robitaille MJ. Comparison of conjunctival autograft transplantation and amniotic membrane transplantation for pterygium: a meta-analysis. Graefe's Archive for Clinical and Experimental Ophthalmology. 2012;250:375-81.
[5] Lim L-A, Madigan MC, Conway RM. Conjunctival melanoma: a review of conceptual and treatment advances. Clinical Ophthalmology (Auckland, NZ). 2013;7:521-31.

[6] Dartt DA, Willcox MDP. Complexity of the tear film: Importance in homeostasis and dysfunction during disease. Experimental eye research. 2013;117:1-3.
[7] Schrader S, Notara M, Beaconsfield M, Tuft SJ, Daniels JT, Geerling G. Tissue engineering for conjunctival reconstruction: established methods and future outlooks. Curr Eye Res. 2009;34:913-24.
[8] Lee SY, Oh JH, Kim JC, Kim YH, Kim SH, Choi JW. In vivo conjunctival reconstruction using modified PLGA grafts for decreased scar formation and contraction. Biomaterials. 2003;24:5049-59.
[9] Hsu WC, Spilker MH, Yannas IV, Rubin PA. Inhibition of conjunctival scarring and contraction by a porous collagen-glycosaminoglycan implant. Invest Ophthalmol Vis Sci. 2000;41:2404-11.
[10] Huang D, Xu B, Yang X, Xu B, Zhao J. Conjunctival structural and functional reconstruction using acellular bovine pericardium graft (Normal GEN(R)) in rabbits. Graefes Arch Clin Exp Ophthalmol. 2016;254:773-83.
[11] Gipson IK. Goblet cells of the conjunctiva: A review of recent findings. Prog Retin Eye Res. 2016;54:49-63.
[12] Zhou H, Lu Q, Guo Q, Chae J, Fan X, Elisseeff JH, et al. Vitrified collagen-based conjunctival equivalent for ocular surface reconstruction. Biomaterials. 2014;35:7398-406.
[13] Barabino S, Rolando M, Bentivoglio G, Mingari C, Zanardi S, Bellomo R, et al. Role of amniotic membrane transplantation for conjunctival reconstruction in ocular-cicatricial pemphigoid. Ophthalmology. 2003;110:474-80.
[14] Kheirkhah A, Ghaffari R, Kaghazkanani R, Hashemi H, Behrouz MJ, Raju VK. A Combined Approach of Amniotic Membrane and Oral Mucosa Transplantation for Fornix Reconstruction in Severe Symblepharon. Cornea. 2013;32:155-60.
[15] Clearfield E, Muthappan V, Wang X, Kuo IC. Conjunctival autograft for pterygium. Cochrane Database Syst Rev. 2016;2:Cd011349.
[16] Morgan PV, Suh JD, Hwang CJ. Nasal Floor Mucosa: New Donor Site for Mucous Membrane Grafts. Ophthalmic Plastic and Reconstructive Surgery. 2016;32:174-7.
[17] Jingbo Liu1, Hosam Sheha1,3, Yao Fu1,4, Lingyi Liang5, and Scheffer CG Tseng. Update on amniotic membrane transplantation. Expert Rev Ophthalmol 2010:5(): 645–61.
[18] Muqit MM, Ellingham RB, Daniel C. Technique of amniotic membrane transplant dressing in the management of acute Stevens-Johnson syndrome. Br J Ophthalmol. 2007;91:1536.
[19] Tamhane A, Vajpayee RB, Biswas NR, Pandey RM, Sharma N, Titiyal JS, et al. Evaluation of amniotic membrane transplantation as an adjunct to medical therapy as compared with medical therapy alone in acute ocular burns. Ophthalmology. 2005;112:1963-9.
[20] Tseng SC. HC-HA/PTX3 Purified From Amniotic Membrane as Novel Regenerative Matrix: Insight Into Relationship Between Inflammation and Regeneration. Invest Ophthalmol Vis Sci. 2016;57:ORSFh1-8.
[21] Liu T, Zhai H, Xu Y, Dong Y, Sun Y, Zang X, et al. Amniotic membrane traps and induces apoptosis of inflammatory cells in ocular surface chemical burn. Mol Vis. 2012;18:2137-46.
[22] Chintan Malhotra AKJ. Human amniotic membrane transplantation: Different modalities of its use in ophthalmology. World J Transplant 2014: 4(2): 111-21.
[23] Manuelpillai U, Moodley Y, Borlongan CV, Parolini O. Amniotic membrane and amniotic cells: potential therapeutic tools to combat tissue inflammation and fibrosis? Placenta. 2011;32 Suppl 4:S320-5.
[24] Yang S, Yang X, Cao G. Conjunctiva reconstruction by induced differentiation of human amniotic epithelial cells. Genet Mol Res. 2015;14:13823-34.
[25] Lopez-Garcia JS, Rivas L, Garcia-Lozano I, Conesa E, Elosua I, Murube J. Amniotic membrane transplantation in acute toxic epidermal necrolysis: histopathologic changes and ocular surface features after 1-year follow-up. Eur J Ophthalmol. 2014;24:667-75.

[26] Shammas MC, Lai EC, Sarkar JS, Yang J, Starr CE, Sippel KC. Management of acute Stevens-Johnson syndrome and toxic epidermal necrolysis utilizing amniotic membrane and topical corticosteroids. Am J Ophthalmol. 2010;149:203-13.e2.
[27] Shay E, Kheirkhah A, Liang L, Sheha H, Gregory DG, Tseng SC. Amniotic membrane transplantation as a new therapy for the acute ocular manifestations of Stevens-Johnson syndrome and toxic epidermal necrolysis. Surv Ophthalmol. 2009;54:686-96.
[28] Barton K, Budenz DL, Khaw PT, Tseng SC. Glaucoma filtration surgery using amniotic membrane transplantation. Invest Ophthalmol Vis Sci. 2001;42:1762-8.
[29] Lee JW, Park WY, Kim EA, Yun IH. Tissue response to implanted Ahmed glaucoma valve with adjunctive amniotic membrane in rabbit eyes. Ophthalmic Res. 2014;51:129-39.
[30] Lu R, Zhang X, Huang D, Huang B, Gao N, Wang Z, et al. Conjunctival Reconstruction with Progenitor Cell-Derived Autologous Epidermal Sheets in Rhesus Monkey. PLOS ONE. 2011;6:e25713.
[31] Marangon FB, Alfonso EC, Miller D, Remonda NM, Muallem MS, Tseng SCG. Incidence of Microbial Infection After Amniotic Membrane Transplantation. Cornea. 2004;23:264-9.
[32] Lee JE, Jun JB, Choi HY, Oum BS, Lee JS. Corneal tattooing to mask subsequent opacification after amniotic membrane grafting for stromal corneal ulcer. Acta Ophthalmol Scand. 2006;84:696-8.
[33] S.P. Yang1 XZYaGPC. Conjunctiva reconstruction by induced differentiation of human amniotic epithelial cellsS.P. Yang1, X.Z. Yang1 and G.P. Ca. brGenetics and Molecular Research 14 (4): 13823-13834 2015:14 (4): 13823-34
[34] Eidet JR, Dartt DA, Utheim TP. Concise Review: Comparison of Culture Membranes Used for Tissue Engineered Conjunctival Epithelial Equivalents. J Funct Biomater. 2015;6:1064-84.
[35] Hsiue GH, Lai JY, Chen KH, Hsu WM. A novel strategy for corneal endothelial reconstruction with a bioengineered cell sheet. Transplantation. 2006;81:473-6.
[36] Lai JY, Chen KH, Hsiue GH. Tissue-engineered human corneal endothelial cell sheet transplantation in a rabbit model using functional biomaterials. Transplantation. 2007;84:1222-32.
[37] Yan J, Qiang L, Gao Y, Cui X, Zhou H, Zhong S, et al. Effect of fiber alignment in electrospun scaffolds on keratocytes and corneal epithelial cells behavior. J Biomed Mater Res A. 2012;100:527-35.
[38] de la Mata A, Nieto-Miguel T, Lopez-Paniagua M, Galindo S, Aguilar MR, Garcia-Fernandez L, et al. Chitosan-gelatin biopolymers as carrier substrata for limbal epithelial stem cells. J Mater Sci Mater Med. 2013;24:2819-29.
[39] Sung B, Shaffer S, Sittek M, Alboslemy T, Kim C, Kim MH. Alternating Magnetic Field-Responsive Hybrid Gelatin Microgels for Controlled Drug Release. J Vis Exp. 2016:53680.
[40] Li Y, Meng H, Liu Y, Narkar A, Lee BP. Gelatin Microgel Incorporated Poly(ethylene glycol)-Based Bioadhesive with Enhanced Adhesive Property and Bioactivity. ACS Appl Mater Interfaces. 2016;8:11980-9.
[41] Lai JY. Corneal stromal cell growth on gelatin/chondroitin sulfate scaffolds modified at different NHS/EDC molar ratios. Int J Mol Sci. 2013;14:2036-55.
[42] Lai JY, Li YT, Cho CH, Yu TC. Nanoscale modification of porous gelatin scaffolds with chondroitin sulfate for corneal stromal tissue engineering. Int J Nanomedicine. 2012;7:1101-14.
[43] Winter H. Can the gel point of a cross-linking polymer be detected by the G'–G "crossover? Polymer Engineering & Science. 1987;27:1698-702.
[44] Djabourov M. Architecture of gelatin gels. Contemporary Physics. 1988;29:273-97.
[45] Picard J, Giraudier S, Larreta-Garde V. Controlled remodeling of a protein-polysaccharide mixed gel: examples of gelatin-hyaluronic acid mixtures. Soft Matter. 2009;5:4198-205.
[46] Harrington JC, Morris ER. Conformational ordering and gelation of gelatin in mixtures with soluble polysaccharides. Food Hydrocolloids. 2009;23:327-36.
[47] Winter HH, Chambon F. Analysis of linear viscoelasticity of a crosslinking polymer at the gel point. Journal of rheology. 1986;30:367-82.

[48] Ferry JD. Viscoelastic properties of polymers: John Wiley & Sons; 1980.
[49] Hyun K, Kim SH, Ahn KH, Lee SJ. Large amplitude oscillatory shear as a way to classify the complex fluids. Journal of Non-Newtonian Fluid Mechanics. 2002;107:51-65.
[50] Rohsenow WM, Hartnett JP, Cho YI. Handbook of heat transfer: McGraw-Hill New York; 1998.
[51] Hsu LC, Fang J, Borca-Tasciuc DA, Worobo RW, Moraru CI. Effect of micro-and nanoscale topography on the adhesion of bacterial cells to solid surfaces. Applied and environmental microbiology. 2013;79:2703-12.
[52] Sammons RL, Lumbikanonda N, Gross M, Cantzler P. Comparison of osteoblast spreading on microstructured dental implant surfaces and cell behaviour in an explant model of osseointegration. Clinical oral implants research. 2005;16:657-66.
[53] Huang H-H, Ho C-T, Lee T-H, Lee T-L, Liao K-K, Chen F-L. Effect of surface roughness of ground titanium on initial cell adhesion. Biomolecular engineering. 2004;21:93-7.
[54] Whitehead KA, Colligon J, Verran J. Retention of microbial cells in substratum surface features of micrometer and sub-micrometer dimensions. Colloids and Surfaces B: Biointerfaces. 2005;41:129-38.
[55] Wenkel H, Rummelt V, Naumann GO. Long term results after autologous nasal mucosal transplantation in severe mucus deficiency syndromes. The British journal of ophthalmology. 2000;84:279-84.
[56] Nakamura T, Inatomi T, Cooper LJ, Rigby H, Fullwood NJ, Kinoshita S. Phenotypic investigation of human eyes with transplanted autologous cultivated oral mucosal epithelial sheets for severe ocular surface diseases. Ophthalmology. 2007;114:1080-8.
[57] Burillon C, Huot L, Justin V, Nataf S, Chapuis F, Decullier E, et al. Cultured autologous oral mucosal epithelial cell sheet (CAOMECS) transplantation for the treatment of corneal limbal epithelial stem cell deficiency. Investigative ophthalmology & visual science. 2012;53:1325-31.
[58] Homma R, Yoshikawa H, Takeno M, Kurokawa MS, Masuda C, Takada E, et al. Induction of epithelial progenitors in vitro from mouse embryonic stem cells and application for reconstruction of damaged cornea in mice. Investigative ophthalmology & visual science. 2004;45:4320-6.
[59] Reinshagen H, Auw-Haedrich C, Sorg RV, Boehringer D, Eberwein P, Schwartzkopff J, et al. Corneal surface reconstruction using adult mesenchymal stem cells in experimental limbal stem cell deficiency in rabbits. Acta ophthalmologica. 2011;89:741-8.
[60] Gomes JA, Geraldes Monteiro B, Melo GB, Smith RL, Cavenaghi Pereira da Silva M, Lizier NF, et al. Corneal reconstruction with tissue-engineered cell sheets composed of human immature dental pulp stem cells. Investigative ophthalmology & visual science. 2010;51:1408-14.
[61] Meyer-Blazejewska EA, Call MK, Yamanaka O, Liu H, Schlotzer-Schrehardt U, Kruse FE, et al. From hair to cornea: toward the therapeutic use of hair follicle-derived stem cells in the treatment of limbal stem cell deficiency. Stem cells (Dayton, Ohio). 2011;29:57-66.
[62] Reza HM, Ng BY, Gimeno FL, Phan TT, Ang LP. Umbilical cord lining stem cells as a novel and promising source for ocular surface regeneration. Stem cell reviews. 2011;7:935-47.
[63] Geggel HS, Friend J, Thoft RA. Conjunctival epithelial wound healing. Investigative ophthalmology & visual science. 1984;25:860-3.
[64] Radford CF, Rauz S, Williams GP, Saw VPJ, Dart JKG. Incidence, presenting features, and diagnosis of cicatrising conjunctivitis in the United Kingdom. Eye. 2012;26:1199-208.
[65] Safinaz MK, Norzana AG, Hairul Nizam MH, Ropilah AR, Faridah HA, Chua KH, et al. The use of autologous fibrin as a scaffold for cultivating autologous conjunctiva in the treatment of conjunctival defect. Cell Tissue Bank. 2014;15:619-26.
[66] Prabhasawat P, Tseng SC. Impression cytology study of epithelial phenotype of ocular surface reconstructed by preserved human amniotic membrane. Arch Ophthalmol. 1997;115:1360-7.
[67] Yang SP, Yang XZ, Cao GP. Conjunctiva reconstruction by induced differentiation of human amniotic epithelial cells. Genet Mol Res. 2015;14:13823-34.

[68] Ahmed Tamer S S MOAK, Waleed M M. Role of Amniotic Membrane Transplantation in Symblepharon. . JOJ Ophthal. 2016;1:555565.
[69] Solomon A, Rosenblatt M, Monroy D, Ji Z, Pflugfelder SC, Tseng SC. Suppression of interleukin 1alpha and interleukin 1beta in human limbal epithelial cells cultured on the amniotic membrane stromal matrix. Br J Ophthalmol. 2001;85:444-9.
[70] Lee H-N, Bernardo R, Han G-Y, Kim G-Y, Kim J-S, Jung W-Y, et al. Human Amniotic Membrane Extracts have Anti-Inflammatory Effects on Damaged Human Corneal Epithelial Cells In Vitro. Journal of Hard Tissue Biology. 2016;25:282-7.
[71] Lee SB, Li DQ, Tan DT, Meller DC, Tseng SC. Suppression of TGF-beta signaling in both normal conjunctival fibroblasts and pterygial body fibroblasts by amniotic membrane. Curr Eye Res. 2000;20:325-34.
[72] Shimmura S, Shimazaki J, Ohashi Y, Tsubota K. Antiinflammatory Effects of Amniotic Membrane Transplantation in Ocular Surface Disorders. Cornea. 2001;20:408-13.
[73] Magatti M, Caruso M, De Munari S, Vertua E, De D, Manuelpillai U, et al. Human Amniotic Membrane-Derived Mesenchymal and Epithelial Cells Exert Different Effects on Monocyte-Derived Dendritic Cell Differentiation and Function. Cell Transplant. 2015;24:1733-52.
[74] Kubo M, Sonoda Y, Muramatsu R, Usui M. Immunogenicity of human amniotic membrane in experimental xenotransplantation. Invest Ophthalmol Vis Sci. 2001;42:1539-46.
[75] Rehg JE, Bush D, Ward JM. The Utility of Immunohistochemistry for the Identification of Hematopoietic and Lymphoid Cells in Normal Tissues and Interpretation of Proliferative and Inflammatory Lesions of Mice and Rats. Toxicologic Pathology. 2012;40:345-74.
[76] Kheirkhah A, Casas V, Sheha H, Raju VK, Tseng SC. Role of conjunctival inflammation in surgical outcome after amniotic membrane transplantation with or without fibrin glue for pterygium. Cornea. 2008;27:56-63.
[77] Li W, He H, Chen YT, Hayashida Y, Tseng SC. Reversal of myofibroblasts by amniotic membrane stromal extract. J Cell Physiol. 2008;215:657-64.
[78] Tseng SC, Li DQ, Ma X. Suppression of transforming growth factor-beta isoforms, TGF-beta receptor type II, and myofibroblast differentiation in cultured human corneal and limbal fibroblasts by amniotic membrane matrix. J Cell Physiol. 1999;179:325-35.
[79] Cooper LJ, Kinoshita S, German M, Koizumi N, Nakamura T, Fullwood NJ. An investigation into the composition of amniotic membrane used for ocular surface reconstruction. Cornea. 2005;24:722-9.